Masked Image Training for Generalizable Deep Image Denoising

Haoyu Chen[1*], Jinjin Gu[2,3*], Yihao Liu[2,4,5], Salma Abdel Magid[6],
Chao Dong[2,4], Qiong Wang[4], Hanspeter Pfister[6], Lei Zhu[1,7†]

[1]The Hong Kong University of Science and Technology (Guangzhou) [2]Shanghai AI Lab [3]The University of Sydney
[4]Shenzhen Institutes of Advanced Technology, Chinese Academy of Sciences [5]University of Chinese Academy of Sciences
[6]Harvard University [7]The Hong Kong University of Science and Technology
Project page: https://github.com/haoyuc/MaskedDenoising

Abstract

When capturing and storing images, devices inevitably introduce noise. Reducing this noise is a critical task called image denoising. Deep learning has become the de facto method for image denoising, especially with the emergence of Transformer-based models that have achieved notable state-of-the-art results on various image tasks. However, deep learning-based methods often suffer from a lack of generalization ability. For example, deep models trained on Gaussian noise may perform poorly when tested on other noise distributions. To address this issue, we present a novel approach to enhance the generalization performance of denoising networks, known as masked training. Our method involves masking random pixels of the input image and reconstructing the missing information during training. We also mask out the features in the self-attention layers to avoid the impact of training-testing inconsistency. Our approach exhibits better generalization ability than other deep learning models and is directly applicable to real-world scenarios. Additionally, our interpretability analysis demonstrates the superiority of our method.

1. Introduction

Image denoising is a crucial research area that aims to recover clean images from noisy observations. Due to the rapid advancements in deep learning, many promising image denoising networks have been developed. These networks are typically trained using images synthesized from a pre-defined noise distribution and can achieve remarkable performance in removing the corresponding noise. However, a significant challenge in applying these deep models to real-world scenarios is their generalization ability. Since the real-world noise distribution can differ from that observed during training, these models often struggle to gen-
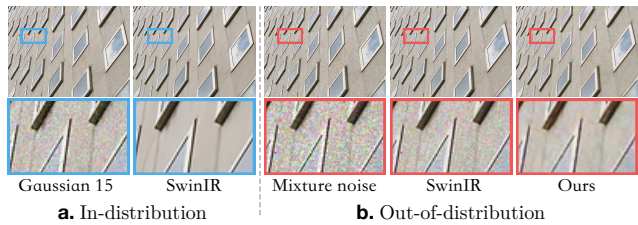

Figure 1. We illustrate the generalization problem of denoising networks. We train a SwinIR model on Gaussian noise with $\sigma = 15$. When tested on the same noise, SwinIR demonstrates outstanding performance. However, when applied to out-of-distribution noise, *e.g.*, the mixture of various noise. SwinIR suffers from a huge performance drop. The model trained by the proposed *masked training* method maintains a reasonable denoising effect, despite aldo being trained on Gaussian noise.

eralize to such scenarios.

More specifically, most existing denoising works train and evaluate models on images corrupted with Gaussian noise, limiting their performance to a single noise distribution. When these models are applied to remove noise drawn from other distributions, their performance drastically drops. Figure 1 shows an example. The research community has become increasingly aware of this generalization issue of deep models in recent years. As a countermeasure, some methods [81] assume that the noise level of a particular noise type is unknown, while others [5, 69] attempt to improve the performance in real-world scenarios by synthesizing or collecting training data closer to the target noise or directly performing unsupervised training on the target noise [11, 72]. However, none of these methods substantially improve the generalization performance of denoising networks, and they still struggle when the noise distribution is mismatched [1]. The generalization issue of deep denoising still poses challenges to making these methods broadly applicable.

In this work, we focus on improving the generalization ability of deep denoising models. We define generalization

---

ability as the model's performance on noise different from what it observed during training. We argue that the generalization issue of deep denoising is due to the overfitting of training noise. The existing training strategy directly optimizes the similarity between the denoised image and the ground truth. The intention behind this is that the network should learn to reconstruct the texture and semantics of natural images correctly. However, what is often overlooked is that the network can also reduce the loss simply by overfitting the noise pattern, which is easier than learning the image content. This is at the heart of the generalization problem. Even many popular deep learning methods exacerbate this overfitting problem. When it comes to noise different from that observed during training, the network exhibits this same behavior, resulting in poor performance.

In light of the preceding discussion, our study seeks to improve the generalization performance of deep denoising networks by directing them to learn image content reconstruction instead of overfitting to training noise. Drawing inspiration from recent masked modeling methods [4, 20, 34, 70], we employ a masked training strategy to explicitly learn representations for image content reconstruction, as opposed to training noise. Leveraging the properties of image processing Transformers [15, 46, 79], we introduce two masking mechanisms: the *input mask* and the *attention mask*. During training, the input mask removes input image pixels randomly, and the network reconstructs the removed pixels. The attention mask is implemented in each self-attention layer of the Transformer, enabling it to learn the completion of masked features dynamically and mitigate the distribution shift between training and testing in masked learning. Although we use Gaussian noise for training – similar to previous works – our method demonstrates significant performance improvements on various noise types, such as speckle noise, Poisson noise, salt and pepper noise, spatially correlated Gaussian noise, Monte Carlo-rendered image noise, ISP noise, and complex mixtures of multiple noise sources. Existing methods and models have yet to effectively and accurately remove all these diverse noise patterns.

2. Related Works

Image Denoising approaches very broadly lie in two categories: traditional model-based and data-driven deep-learning-based. Traditional methods are usually based on modeling image priors to recover image content contaminated by noise [7, 19, 23, 32, 54]. These methods usually do not impose too many constraints on the type of noise, and have been proven to be applicable to a variety of noise, with good generalization performance [1]. However, these methods are not satisfactory for the reconstruction of image content. In recent years, the paradigm of denoising has gradually shifted to data-driven methods based on deep

learning methods [13]. Many techniques have been proposed to improve the capabilities of the denoising networks continuously, *e.g.*, residual networks [39, 81, 82], dense networks [37, 87], recursive networks [9, 49, 64], multi-scale [21, 31, 77], encoder-decoder [16, 55, 74], attention operations [85, 86], self-similarity [35], and non-local operations [44, 45, 59]. Since 2020, the paradigm of vision network design has gradually shifted from CNNs to Transformers [22]. Vision Transformers treat input pixels as tokens and use self-attention operations to process interactions between these tokens. Inspired by the success of vision Transformers, many attempts have been made to employ Transformers for low-level vision tasks [10, 14, 15, 46, 63, 68, 71, 75, 78, 79] During the development of these models, the noise pattern used for training is often consistent with the testing one. The factor that determines its denoising performance is the fitting ability of the network, in other words, the ability of the network to overfit to the training noise. However, a better network does not mean a better generalization ability of the denoising model. As we will show in the experiment section, a more efficient network even indicates worse generalization performance.

Generalization Problem in low-level vision often arises when the testing degradation does not match the training degradation, *e.g.*, different downsampling kernel in super-resolution [30, 40, 48]. We typically develop deep denoising models based on Gaussian noise in the laboratory setting. However, noise in the real-world is mostly non-Gaussian. Models trained on Gaussian noise fail in these non-Gaussian scenarios. There are two main categories of solutions to this problem. The first is to make training datasets with noise modeling as close to reality as possible during development, *e.g.*, synthesizing real noise according to physical system modeling [5, 69], learning to generate real noise [11, 24, 72], collecting real noise – clean image pairs for training [1, 33, 42, 58]. Although the models obtained by these methods can improve the effect on the target noise, they still cannot generalize to out-of-distribution noise. Another category of solutions is to develop "blind" denoising models, which are supposed to deal with unknown noise [42, 73, 81]. These methods usually simply assume that the noise level is unknown, or train on a large amount of noise types [80], which also fails to generalize to other noise not present in the training set. Few workd have been proposed to study the reasons for the lack of generalization ability in low-level vision [40]. Liu *et al*. [50] argue that networks tend to overfit to degradations and show degradation "semantics" inside the network. The presence of these representations often means a decrease in generalization ability. The utilization of this knowledge can guide us to analyze and evaluate the generalization performance [51]. Apart from that, few works have been proposed to improve the generalization ability of denoising models.
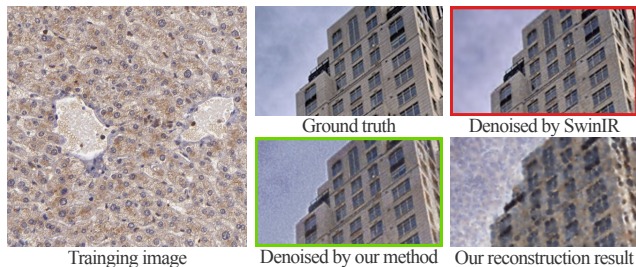
Figure 2. SwinIR, when trained solely on immunohistochemistry images with Gaussian noise, can still denoise natural images. This observation supports the assertion that most existing methods perform denoising primarily through overfitting the training noise. In contrast, our approach emphasizes reconstructing natural image textures and edges observed in the training set on natural images, rather than relying on noise overfitting for denoising. This distinction underlines the fundamental difference between our method and previous approaches. "Our reconstruction result" refers to using our model but taking masked images as input.
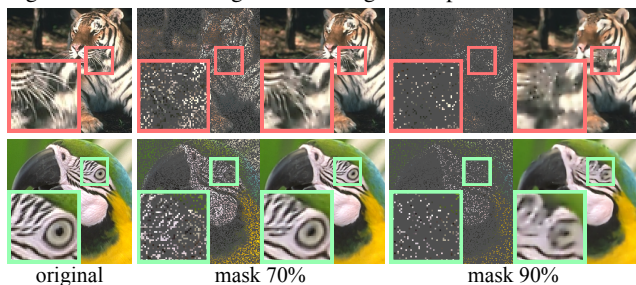

Figure 3. The illustration of the proposed mask-and-complete training strategy. Even if a large number of pixels are masked, the model can still reconstruct the input to some extent.

Masked modeling for language [6, 20, 60, 61] is successful for learning pre-trained representations that generalize well to various downstream tasks. These methods mask out a portion of the input sequence and train models to predict the missing content. A similar approach can also be applied to the vision model pre-training. Masked image models learn representations from corrupted images. The earliest attempts in this regard can be traced back at least to the denoising auto-encoder [67]. Since then, many works have used predicting missing parts of images to learn efficient image representations [4, 12, 34, 57, 70]. However, there have been few successful attempts to apply masked image modeling to low-level vision, even though the masked pre-training method is in the form of low-level vision tasks.

3. Method

Our objective is to create denoising models capable of generalizing to noise not encountered in the training set. In this section, we first discuss our motivation before delving into the specifics of our masked training method.

Motivation. When training a deep network on a large number of images, the expectation is for the network to learn to discern the rich semantics of natural images from noise-contaminated test cases. However, several studies have noted that the semantics and knowledge acquired by low-level vision networks differ significantly from our expectations [29, 50, 51, 53]. We argue that the poor generalization ability of denoising models results from our training method, which leads the model to *focus on overfitting the training noise rather than learning image reconstruction*. We conduct a simple experiment for verification. We trained a SwinIR denoising network [46] using images that greatly differ from natural images (immunohistochemistry images [66]). We synthesized training data pairs using Gaussian noise, and then assessed the model's performance on *natural images* with Gaussian noise. According to our hypothesis, if the model learns the content and reconstruction of image semantics from the training set, it should not perform well on natural images, as it has not been exposed to any. If the model is simply overfitting the noise, the model can remove the noise even if the images are different, as the model mainly relies on detecting the noise for denoising.

The results are presented in Figure 2. As observed, the SwinIR trained on immunohistochemistry images can still denoise and reproduce the natural image. This supports our conjecture regarding generalization ability, indicating that most existing methods perform denoising by overfitting the training noise. Consequently, when the noise deviates from the training conditions, the denoising performance of these models declines significantly.

This observation also inspires our approach to developing deep denoising models with improved generalization ability. We aim for the model to learn the reconstruction of image textures and structures, rather than focusing only on noise. In this paper, we propose a new masked training strategy for denoising networks. During training, we mask out a portion of the input pixels and then train the deep network to complete them, as shown in Figure 3. Our approach emphasizes reconstructing natural image textures and edges observed in the image, rather than overfitting noise. In Figure 2 we also show the results of our method. It is evident that our approach seeks to reconstruct the immuno-histochemistry image texture from the training set on the testing natural image, instead of relying on noise overfitting for denoising. This demonstrates the potential of this idea in improving generalization performance. By training our method on natural images, it will concentrate on reconstructing the content of natural images, aligning with our core concept of employing deep learning for low-level vision tasks.

The Transformer Architecture. Our approach exploits the excellent properties of visual Transformers, so we first describe the basic Transformer backbone used in this study. The shifted window mechanism is proven to be flexible and
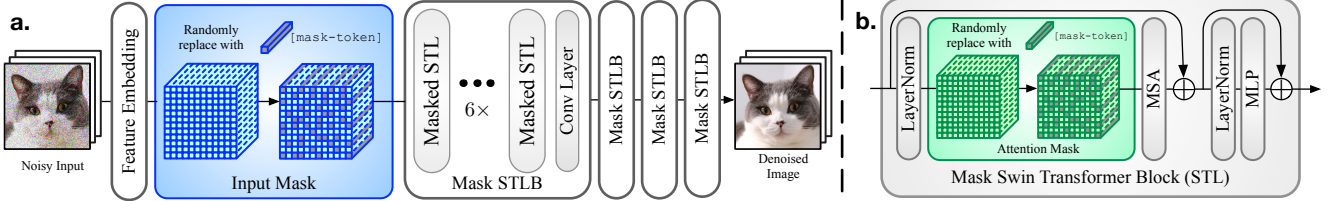
Figure 4. The transformer architecture of our proposed masked image training. We make a minimal change to the original SwinIR architecture – the input mask operation and the attention masks. Other micro-designs are not essentially different from other Transformers.
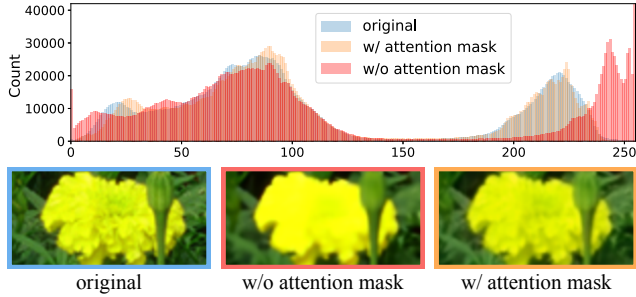

Figure 5. Quantitative effect of the attention mask. The histogram differences are also shown above.

Mixture noise   w/o input mask w/o attention mask   full method   Reference

Figure 6. The effectiveness of the input mask and attention mask. Note that the brightness of the image is wrong *w/o* attention mask.

Input Mask	Attention Mask	PSNR	SSIM
	✓	29.17	0.8227
✓		26.96	0.8202
✓	✓	**29.74**	**0.8672**

Table 1. The importance of using different mask operations.

Mix. noise on CBSD68 [56]		
Ratio (%)	PSNR	SSIM
65	29.57	0.8657
75	**29.76**	**0.8678**
85	28.84	0.8548

Table 2. Ablation on the attention mask ratio.

effective for image processing tasks [15, 46, 79]. We only make minimal changes when applying it to the proposed masked training method without the loss of generality. This model is illustrated in Figure 4. Transformers divide the input signal into tokens and process spatial information using self-attention layers. In our method, a convolution layer with kernel size 1 is used as the feature embedding module to project the 3-channel pixel values into C-dimensional feature tokens. The 1×1 convolution layer ensures that pixels do not affect each other during feature embedding, which facilitates subsequent masking operations. These feature tokens are gathered with shape $H \times W \times C$, where H, W and C are the height, width and feature dimension. The shifted window mechanism first reshapes the feature maps of each frame to $\frac{HW}{M^2} \times M^2 \times C$ features by partitioning the input into non-overlapping $M \times M$ local windows, where $\frac{HW}{M^2}$ is the total number of windows. We calculate self-attention on the feature tokens within the same window. Therefore, M^2 tokens are involved in each standard self-attention operation, and we produce the local window feature $X \in \mathbb{R}^{M^2 \times C}$. In each self-attention layer, the query Q, key K and value V are calculated as $Q = XW^Q$, $K = XW^K$, $V = XW^V$, where $W^Q, W^K, W^V \in \mathbb{R}^{C \times D}$ are weight matrices, and D is the dimension of projected vectors. Then, we use Q to query K to generate the attention map $A = \texttt{softmax}(QK^T/\sqrt{D} + B) \in \mathbb{R}^{M^2 \times M^2}$, where B is the learnable relative positional encoding. This attention map A is then used for the weighted sum of M^2 vectors in V. The multi-head settings are aligned with SwinIR [46] and ViT [22].

Masked Training. Our masked training mainly consists of two aspects, the input mask and the attention mask. Although both are mask operations, the purpose of these two masks is different. We describe them separately.

The Input Mask randomly masks out the feature tokens embedded by the first convolution layer, and encourages the network to complete the masked information during training. The input mask explicitly constructs a very challenging inpainting problem, as shown in Figure 3. It can be seen that even if up to 90% of the pixel information is destroyed, the network can still reconstruct the target image to a certain extent. The method is very simple. Given the feature token tensor $\mathbf{f} \in \mathbb{R}^{H \times W \times C}$, we randomly replace the token with a [mask token]$\in \mathbb{R}^C$ with a probability p_{IM}, where p_{IM} is called the input mask ratio. The network is trained under the supervision of the l_1-norm of the reconstructed image and the ground truth. The [mask token] can be learnable and initialized with a $\mathbf{0}$ vector. But we actually found that the $\mathbf{0}$ vector itself is already a suitable choice. The existence of the input mask forces the network to learn to recognize and reconstruct the content of the image from very limited information.

The Attention Mask. We cannot build usable image processing networks relying solely on the input mask operation. Because during testing, we will input uncorrupted images to retain enough information. At this time, due to the inconsistency between training and testing, the network will tend to increase the brightness of the output image. Such as the example in Figure 5. Since Transformer uses the self-
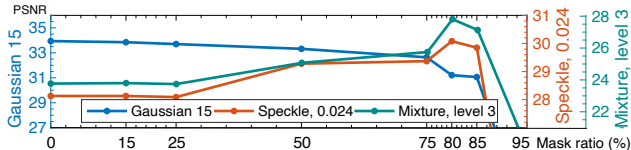
Figure 7. The trade-off of choosing different mask ratios. The performance drop on training noise is not significant until 75% masking ratio. Our performance gain on the noise outside the training set is greater than the performance loss on the training set.

attention operation to process spatial information, we can narrow the gap between training and testing by performing the same mask operation during the self-attention process. The specific mask operation is similar to the input mask, but a different attention mask ratio p_{AM} and [mask token] are used. When some tokens in the self-attention are masked, the attention operation will adjust to the fact that the information of these tokens is no longer reliable. Self-attention will focus on unmasked tokens in each layer and complete the masked information. This operation is difficult to implement on convolutional networks. Figure 5 shows the effect of the attention mask. As can be seen, the attention mask successfully makes the masked trained network work on the unmasked input image.

4. Experiments

Training Settings. For synthesizing training data, we sample the clean images from DIV2K [65], Flickr2K [47], BSD500 [3], and WED [52] during training. In our work, all the networks are trained using Gaussian noise with standard deviation $\sigma = 15$. Each input image is randomly cropped to a spatial resolution of 64×64, and the number of the total training iteration is 200K. We adopt the Adam optimizer [38] with β_1=0.9 and β_2=0.99 to minimize the L_1 pixel loss. The initial learning rate is set as 1×10^{-4} and reduced by half at the milestone of 100K iterations and 150K iterations. The batch size is set to 64.

Testing Noise. Since the training process utilizes the Gaussian noise, we evaluate the generalization performance of the models on six other synthetic noise: (1) Speckle noise, a type of noise that occurs during the acquisition of medical images or tomography images. (2) Poisson noise, a type of signal-dependent noise that occurs during the acquisition of digital images. (3) Spatially-correlated noise. This is to synthesize the complex artifact after denoising using a flawed algorithm. It is produced by filtering Gaussian noise with a 3×3 average kernel. Different standard deviations of the Gaussian noise indicate different noise levels. (4) Salt & pepper noise. (5) Image signal processing (ISP) noise. [5] proposes a method to synthesize realistic ISP noise during digital imaging. (6) Mixture noise obtained by mixing the above different types of noise with different levels [80]. The clean images are sampled from the bench-

mark datasets, including CBSD68 [56], Kodak24 [26], Mc-Master [83], and Urban100 [36]. We also include two real noise types in this work: the Smartphone Image Denoising Dataset (SIDD) [1] and Monte Carlo (MC) rendered image noise. For evaluation, we follow [27,28] and use the metrics PSNR, SSIM [52], and LPIPS [84] to evaluate the results. Since PSNR and SSIM are questioned in assessing the perceptual quality of images [27,28], we also use the LPIPS as an additional metric.

4.1. Resutls

Ablation Study. Table 1 and Figure 6 show the effectiveness of using different mask operations. As we can see, without the input mask, the model will lose its generalization ability, and cannot effectively remove the noise outside the training set. Without the attention mask, due to the training-testing inconsistency, the quantitative performance degrades significantly, and the output image will have the wrong brightness. In addition, even without the attention mask, the generalization ability of the model is not significantly affected, and most of the noise is still effectively removed. The input mask is the crucial factor in improving the model the generalization ability.

Table 3a shows the impact of the different input mask ratios. We test fixed ratios and random ratios from a uniform distribution. From our experiments, fixed ratios are less stable for training than randomly chosen from a range, and the performance is also worse. The best quantitative performance is achieved with random sampling ratios between 75% ∼ 85%. This is a trade-off between denoising generalization ability and the preservation of image details. As shown in Figure 7, smaller ratios are not enough for the network to learn the distribution of images because more noise patterns are preserved. The larger ratio improves the model generalization, as the model focuses more on reconstruction. But at the same time, some image details may be lost. For attention mask ratio, we show the effects in Table 2. The optimal ratios are around 75%.

The Generalization Performance. We evaluate our deep denoising method on synthetic noise, where our training noise follows a Gaussian distribution with a single noise level, but we test on multiple types of non-Gaussian noise to assess the model's generalization performance. In Figure 11, we compare our method with other state-of-the-art models based on their PSNR and SSIM scores. The results show that our model outperforms all the other models in terms of generalization performance. Particularly, as the noise level increases, our model exhibits a slower performance degradation and thus demonstrates better generalization. In contrast, other models suffer from significant performance drops when dealing with more severe noise. We also provide visual comparisons in Figure 8, where our model achieves remarkable denoising results even though it
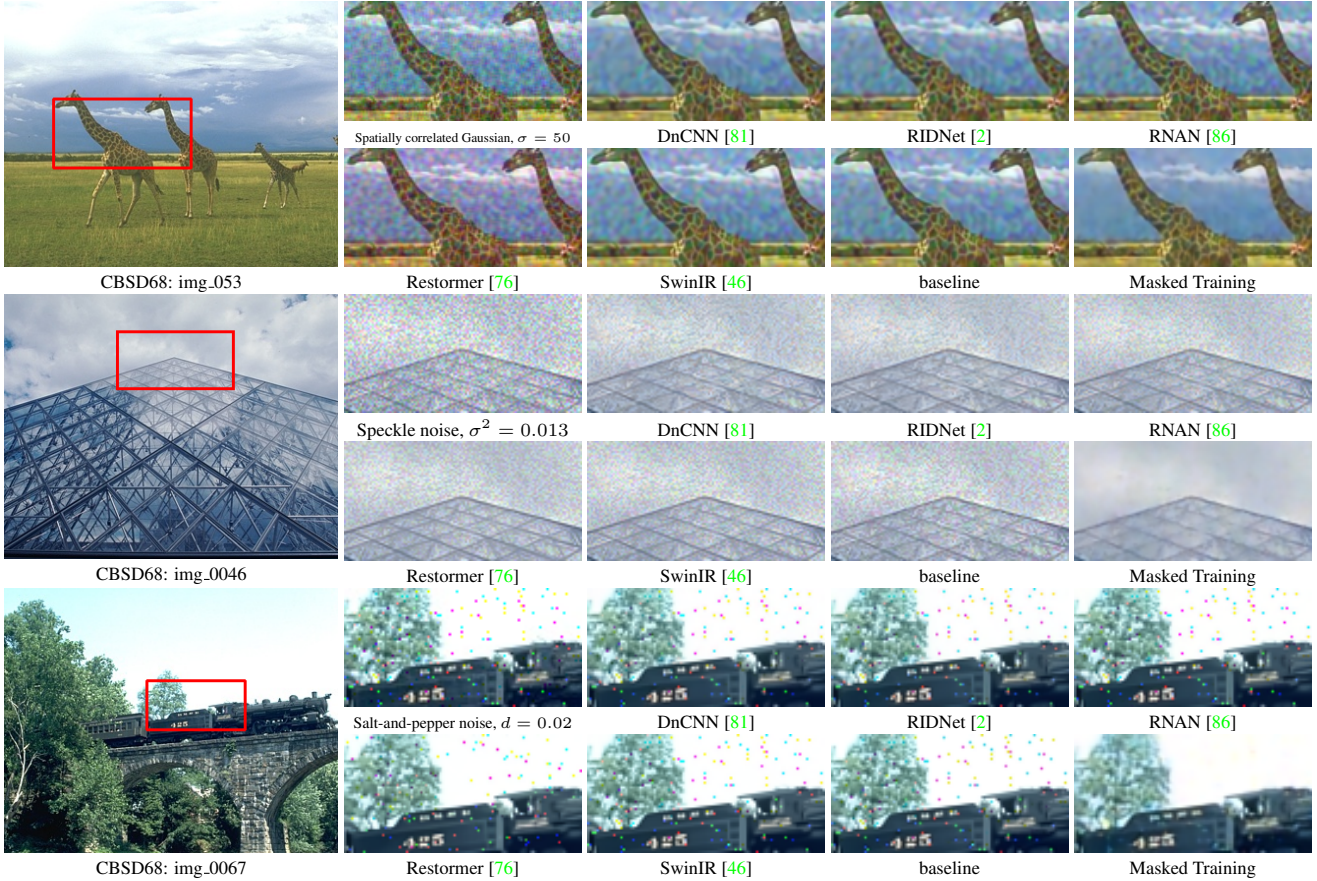
Figure 8. Visual comparison on out-of-distribution noise. When all other methods fail completely, our method is still able to denoise effectively. Please refer to the supplementary material to see more visual results.
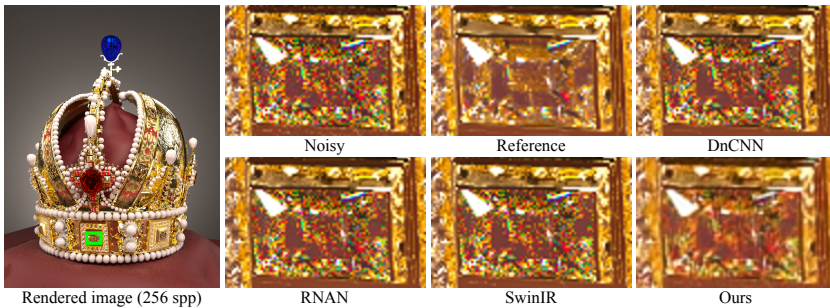
Figure 9. Visual results of denoising a Monte Carlo rendered image.
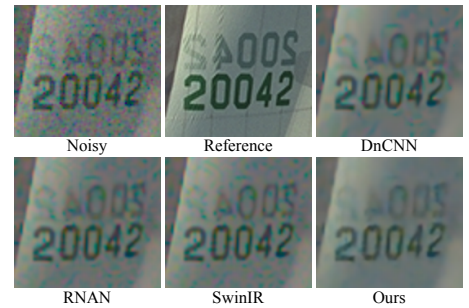
Figure 10. Results of ISP noise removal.

is trained only on Gaussian noise with a fixed standard deviation. In contrast, existing models tend to overfit the training noise and fail when facing unseen noise. More quantitative and qualitative results can be found in the supplementary material.

Evaluation on ISP noise. The removal of the ISP noise is of great application value. Brooks *et al.* [5] present a systematic approach for generating realistic raw data with ISP noise that can facilitate our research. We use the default parameter settings of the method proposed in [5] to synthesize ISP noise on the Kodak24 [26] dataset for testing. The results are shown in Figure 10 and Table 3c. Our method

achieves superior results compared to all other methods. Notably, our method achieves a significant lead in LPIPS, indicating that our results exhibit better perceptual quality. Although DnCNN and our method obtain the same PSNR, our method still outperforms DnCNN in terms of SSIM and LPIPS. Furthermore, as evident from Figure 10, DnCNN's results still contain visible noise, while our method effectively removes the noise.

Evaluation on Monte Carlo rendering noise. Monte Carlo denoising is a vital component of the rendering process since the widespread use in the industry of Monte Carlo rendering algorithms [8, 17, 43]. We use the test dataset

6

(a) Abl. of input mask ratios.

Mix. noise on CBSD68 [56]		
Ratio (%)	PSNR	SSIM
75	29.17	0.8132
85	29.44	0.8545
95	19.60	0.7273
70–80	29.86	0.8593
75–85	**30.04**	**0.8756**
75–90	29.87	0.8728
75–95	29.26	0.8607
80–90	29.74	0.8672

(b) Quantitative comparison on Monte Carlo rendered image denoising.

Method	128 samples per pixel			64 samples per pixel		
	PSNR	SSIM	LPIPS	PSNR	SSIM	LPIPS
DnCNN [81]	29.94	0.7883	0.2671	26.28	0.6779	0.4216
RIDNet [2]	29.96	0.7921	0.2548	26.27	0.6788	0.4122
RNAN [86]	29.86	0.7825	0.2702	26.26	0.6743	0.4290
SwinIR [46]	29.32	0.7627	0.2943	26.14	0.6651	0.4485
Restormer [76]	24.98	0.6598	0.4575	24.59	0.5880	0.5375
Dropout [40]	28.85	0.7753	0.2941	26.10	0.6696	0.4443
baseline	29.68	0.7738	0.2851	25.91	0.6535	0.4564
Ours	**30.62**	**0.8500**	**0.2254**	**28.25**	**0.7694**	**0.3348**

(c) Comparison on synthetic ISP noise.

Method	Synthetic ISP noise [5]		
	PSNR	SSIM	LPIPS
DnCNN [81]	**29.44**	0.7857	0.3083
RIDNet [2]	28.75	0.7446	0.3696
RNAN [86]	28.47	0.7243	0.3601
SwinIR [46]	28.39	0.7079	0.3346
Restormer [76]	19.31	0.4982	0.6556
Dropout [40]	28.39	0.7816	0.2621
baseline	28.89	0.7595	0.2917
Ours	**29.44**	**0.7920**	**0.2368**

Table 3. We train all the models on Gaussian noise, $\sigma = 15$. All the testing noise is out of the training set, therefore the results can show the models' generalization performance on different unseen noise.
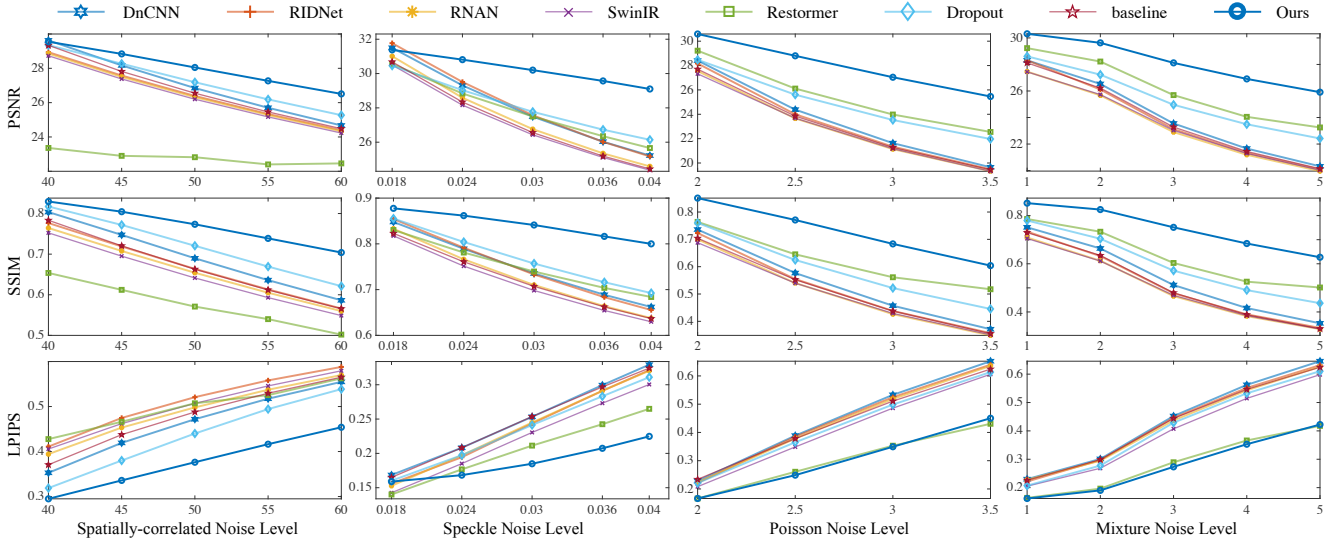
Figure 11. Performance comparisons on four noise types with different levels on the Kodak24 dataset [26]. All models are trained only on Gaussian noise. Our masked training approach demonstrates good generalization performance across different noise types. We involve multiple types and levels of noise in testing, the results cannot be shown here. More results are shown in the supplementary material.

proposed by [25] for Monte Carlo rendered image denoising. The test images were rendered in 128 samples-per-pixel (spp) and 64 spp. The lower the spp, the more severe the noise of the image. In order to adapt the test set to our model, we first convert the data set to sRGB color space by tone mapping. Figure 9 and Table 3b show the denoising results. Our method outperforms all methods on both 128spp and 64spp settings. In Figure 9, the existing methods fail completely because of poor generalization. Our model is still able to remove this noise, demonstrating the wide applicability of our method.

4.2. Generalization Analysis

Training curve. Figure 13 shows the training curves of the model with and without the proposed masked training. The models are trained using only Gaussian noise. The baseline method has a significant overfitting problem. The performance of our method gradually improves with training without overfitting.

CKA analysis. To investigate how masked training differs from normal training strategy, we utilize the centered kernel alignment (CKA) [18, 62] to analyze the differences between network representations obtained from those two training methods. Due to the limited space, we describe the detail of CKA in supplementary. In Figure 12, we present our key findings. Specifically, Figure 12 (a) shows the cross-model comparison between the baseline model and our masked training model. We observe a significant difference between the two models in terms of their feature correlations in the deeper layers. Specifically, the features of the deeper layers of the baseline model exhibit low correlations with all layers of our model. This finding suggests that these two training methods exhibit inconsistent learning patterns for features, especially for the deeper layers.

To explore how the models perform on different noise types, Figure 12 (b) shows the cross-noise comparison between in-distribution noise and out-of-distribution noise, such as Gaussian and Poisson noise. For the baseline model, we observe a low correlation between different noise types

a. cross-model comparison on Gaussian 15

b. cross-model comparison between different noise
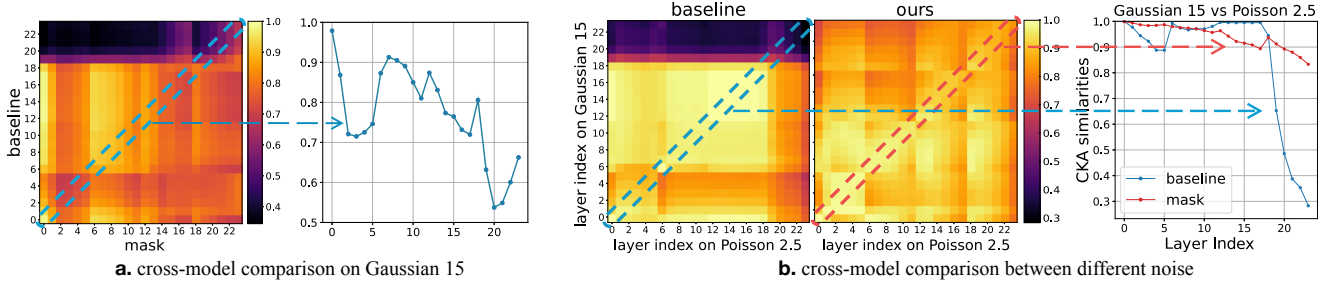
Figure 12. CKA similarity to analyze the representation similarity of network layers.
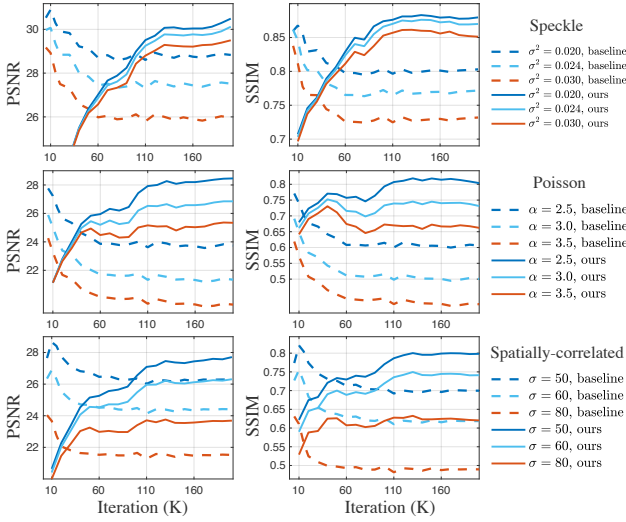
Figure 13. The testing curves on different noise types and levels.
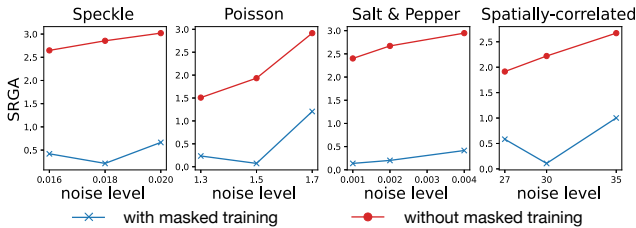
Figure 14. Comparing generalization ability with the SRGA metric. A lower SRGA value indicates better generalization ability.
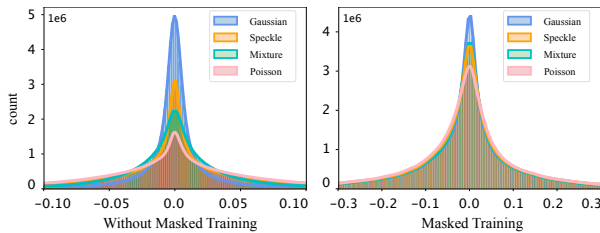
Figure 15. The distribution of baseline model features is biased across different noise types. Our method produces similar feature distributions across different noise.

in the deep layers, indicating that the network processes these two types of noise in different ways for the deep layers. This trend holds for other types of noise as well. This

phenomenon may be due to the baseline approach causing the deep layers of the model to overfit to the patterns of the training set, thereby limiting their generalization capabilities to handle different noise types. In contrast, the high correlation between adjacent layers in our masked training model suggests that the model's representation of the two different noise types is similar. The proposed masked training forces the network to learn the underlying distribution of the images themselves, which makes the model more robust to different types of noise and enhances its generalization capability.

Quantification of generalization performance. Liu *et al.* [50, 51] suggest that model generalization ability can be measured by measuring the consistency of the model's representations across different types of noise. They also propose a generalization assessment index for low-level vision networks called SRGA [51]. It is a non-parametric and non-learning metric which exploits the statistical characteristics of internal features of deep networks. The lower the value of SRGA, the better the generalization ability. In our case, we use Gaussian noise as the reference and other types of noise for testing. Figure 14 shows the SRGA results. Inspired by [51], we visualize the distributions of deep features on different noise types, shown in Figure 15. We can see that for the baseline model, the feature distributions under different noise types deviate from each other significantly. For the model *w/* masked training, the deep feature distributions of different noise types are close to each other. This confirms the effectiveness of our method.

5. Conclusion and Limitations

In summary, our masked training method provides a promising approach to improving the generalization performance of deep learning-based image denoising models. The limitation of our method is that the mask operation inevitably loses information. How to preserve more details needs to be explored in future work. Our approach is a step towards developing more robust models for real-world applications.

References

[1] Abdelrahman Abdelhamed, Stephen Lin, and Michael S Brown. A high-quality denoising dataset for smartphone cameras. In *Proceedings of the IEEE Conference on Computer Vision and Pattern Recognition*, pages 1692–1700, 2018. 1, 2, 5, 13, 14

[2] Saeed Anwar and Nick Barnes. Real image denoising with feature attention. In *Proceedings of the IEEE/CVF international conference on computer vision*, pages 3155–3164, 2019. 6, 7, 13, 16, 17, 18, 19, 20

[3] Pablo Arbelaez, Michael Maire, Charless Fowlkes, and Jitendra Malik. Contour detection and hierarchical image segmentation. *TPAMI*, 2010. 5

[4] Hangbo Bao, Li Dong, and Furu Wei. Beit: Bert pre-training of image transformers. *arXiv preprint arXiv:2106.08254*, 2021. 2, 3

[5] Tim Brooks, Ben Mildenhall, Tianfan Xue, Jiawen Chen, Dillon Sharlet, and Jonathan T Barron. Unprocessing images for learned raw denoising. In *Proceedings of the IEEE/CVF Conference on Computer Vision and Pattern Recognition*, pages 11036–11045, 2019. 1, 2, 5, 6, 7, 13

[6] Tom Brown, Benjamin Mann, Nick Ryder, Melanie Subbiah, Jared D Kaplan, Prafulla Dhariwal, Arvind Neelakantan, Pranav Shyam, Girish Sastry, Amanda Askell, et al. Language models are few-shot learners. *Advances in neural information processing systems*, 33:1877–1901, 2020. 3

[7] Antoni Buades, Bartomeu Coll, and J-M Morel. A non-local algorithm for image denoising. In *2005 IEEE computer society conference on computer vision and pattern recognition (CVPR'05)*, volume 2, pages 60–65. Ieee, 2005. 2

[8] Brent Burley, David Adler, Matt Jen-Yuan Chiang, Hank Driskill, Ralf Habel, Patrick Kelly, Peter Kutz, Yining Karl Li, and Daniel Teece. The design and evolution of disney's hyperion renderer. *ACM Transactions on Graphics (TOG)*, 37(3):1–22, 2018. 6

[9] Chang Chen, Zhiwei Xiong, Xinmei Tian, and Feng Wu. Deep boosting for image denoising. In *Proceedings of the European Conference on Computer Vision (ECCV)*, pages 3–18, 2018. 2

[10] Hanting Chen, Yunhe Wang, Tianyu Guo, Chang Xu, Yiping Deng, Zhenhua Liu, Siwei Ma, Chunjing Xu, Chao Xu, and Wen Gao. Pre-trained image processing transformer. In *CVPR*, 2021. 2

[11] Jingwen Chen, Jiawei Chen, Hongyang Chao, and Ming Yang. Image blind denoising with generative adversarial network based noise modeling. In *Proceedings of the IEEE conference on computer vision and pattern recognition*, pages 3155–3164, 2018. 1, 2

[12] Mark Chen, Alec Radford, Rewon Child, Jeffrey Wu, Heewoo Jun, David Luan, and Ilya Sutskever. Generative pretraining from pixels. In *International conference on machine learning*, pages 1691–1703. PMLR, 2020. 3

[13] Yunjin Chen and Thomas Pock. Trainable nonlinear reaction diffusion: A flexible framework for fast and effective image restoration. *IEEE transactions on pattern analysis and machine intelligence*, 39(6):1256–1272, 2016. 2

[14] Zheng Chen, Yulun Zhang, Jinjin Gu, Linghe Kong, and Xiaokang Yang. Recursive generalization transformer for image super-resolution. *arXiv preprint arXiv:2303.06373*, 2023. 2

[15] Zheng Chen, Yulun Zhang, Jinjin Gu, Yongbing Zhang, Linghe Kong, and Xin Yuan. Cross aggregation transformer for image restoration. In *NIPS*, 2022. 2, 4

[16] Shen Cheng, Yuzhi Wang, Haibin Huang, Donghao Liu, Haoqiang Fan, and Shuaicheng Liu. Nbnet: Noise basis learning for image denoising with subspace projection. In *Proceedings of the IEEE/CVF Conference on Computer Vision and Pattern Recognition*, pages 4896–4906, 2021. 2

[17] Per Christensen, Julian Fong, Jonathan Shade, Wayne Wooten, Brenden Schubert, Andrew Kensler, Stephen Friedman, Charlie Kilpatrick, Cliff Ramshaw, Marc Bannister, et al. Renderman: An advanced path-tracing architecture for movie rendering. *ACM Transactions on Graphics (TOG)*, 37(3):1–21, 2018. 6

[18] Corinna Cortes, Mehryar Mohri, and Afshin Rostamizadeh. Algorithms for learning kernels based on centered alignment. *The Journal of Machine Learning Research*, 13:795–828, 2012. 7, 15

[19] Kostadin Dabov, Alessandro Foi, Vladimir Katkovnik, and Karen Egiazarian. Image denoising by sparse 3-d transform-domain collaborative filtering. *IEEE Transactions on image processing*, 16(8):2080–2095, 2007. 2

[20] Jacob Devlin, Ming-Wei Chang, Kenton Lee, and Kristina Toutanova. Bert: Pre-training of deep bidirectional transformers for language understanding. *arXiv preprint arXiv:1810.04805*, 2018. 2, 3

[21] Nithish Divakar and R Venkatesh Babu. Image denoising via cnns: An adversarial approach. In *Proceedings of the IEEE Conference on Computer Vision and Pattern Recognition Workshops*, pages 80–87, 2017. 2

[22] Alexey Dosovitskiy, Lucas Beyer, Alexander Kolesnikov, Dirk Weissenborn, Xiaohua Zhai, Thomas Unterthiner, Mostafa Dehghani, Matthias Minderer, Georg Heigold, Sylvain Gelly, et al. An image is worth 16x16 words: Transformers for image recognition at scale. *arXiv preprint arXiv:2010.11929*, 2020. 2, 4

[23] Michael Elad and Michal Aharon. Image denoising via sparse and redundant representations over learned dictionaries. *IEEE Transactions on Image processing*, 15(12):3736–3745, 2006. 2

[24] Ruicheng Feng, Jinjin Gu, Yu Qiao, and Chao Dong. Suppressing model overfitting for image super-resolution networks. In *Proceedings of the IEEE/CVF Conference on Computer Vision and Pattern Recognition Workshops*, pages 0–0, 2019. 2

[25] Arthur Firmino, Jeppe Revall Frisvad, and Henrik Wann Jensen. Progressive denoising of monte carlo rendered images. In *Computer Graphics Forum*, volume 41, pages 1–11. Wiley Online Library, 2022. 7, 13

[26] Rich Franzen. Kodak lossless true color image suite. source: http://r0k.us/graphics/kodak/, 1999. 5, 6, 7, 15, 17

[27] Jinjin Gu, Haoming Cai, Haoyu Chen, Xiaoxing Ye, Jimmy Ren, and Chao Dong. Image quality assessment for perceptual image restoration: A new dataset, benchmark and metric. *arXiv preprint arXiv:2011.15002*, 2020. 5

[28] Jinjin Gu, Haoming Cai, Haoyu Chen, Xiaoxing Ye, Jimmy Ren, and Chao Dong. Pipal: a large-scale image quality assessment dataset for perceptual image restoration. In *European Conference on Computer Vision*, pages 633–651. Springer, 2020. 5

[29] Jinjin Gu and Chao Dong. Interpreting super-resolution networks with local attribution maps. In *Proceedings of the IEEE/CVF Conference on Computer Vision and Pattern Recognition*, pages 9199–9208, 2021. 3

[30] Jinjin Gu, Hannan Lu, Wangmeng Zuo, and Chao Dong. Blind super-resolution with iterative kernel correction. In *Proceedings of the IEEE/CVF Conference on Computer Vision and Pattern Recognition*, pages 1604–1613, 2019. 2

[31] Shuhang Gu, Yawei Li, Luc Van Gool, and Radu Timofte. Self-guided network for fast image denoising. In *Proceedings of the IEEE/CVF International Conference on Computer Vision*, pages 2511–2520, 2019. 2

[32] Shuhang Gu, Lei Zhang, Wangmeng Zuo, and Xiangchu Feng. Weighted nuclear norm minimization with application to image denoising. In *Proceedings of the IEEE conference on computer vision and pattern recognition*, pages 2862–2869, 2014. 2

[33] Shi Guo, Zifei Yan, Kai Zhang, Wangmeng Zuo, and Lei Zhang. Toward convolutional blind denoising of real photographs. In *Proceedings of the IEEE/CVF conference on computer vision and pattern recognition*, pages 1712–1722, 2019. 2

[34] Kaiming He, Xinlei Chen, Saining Xie, Yanghao Li, Piotr Dollár, and Ross Girshick. Masked autoencoders are scalable vision learners. In *Proceedings of the IEEE/CVF Conference on Computer Vision and Pattern Recognition*, pages 16000–16009, 2022. 2, 3

[35] Xiaowan Hu, Ruijun Ma, Zhihong Liu, Yuanhao Cai, Xiaole Zhao, Yulun Zhang, and Haoqian Wang. Pseudo 3d autocorrelation network for real image denoising. In *Proceedings of the IEEE/CVF Conference on Computer Vision and Pattern Recognition*, pages 16175–16184, 2021. 2

[36] Jia-Bin Huang, Abhishek Singh, and Narendra Ahuja. Single image super-resolution from transformed self-exemplars. In *CVPR*, 2015. 5, 15, 20

[37] Xixi Jia, Sanyang Liu, Xiangchu Feng, and Lei Zhang. Focnet: A fractional optimal control network for image denoising. In *Proceedings of the IEEE/CVF Conference on Computer Vision and Pattern Recognition*, pages 6054–6063, 2019. 2

[38] Diederik Kingma and Jimmy Ba. Adam: A method for stochastic optimization. In *ICLR*, 2015. 5

[39] Filippos Kokkinos and Stamatios Lefkimmiatis. Deep image demosaicking using a cascade of convolutional residual denoising networks. In *Proceedings of the European conference on computer vision (ECCV)*, pages 303–319, 2018. 2

[40] Xiangtao Kong, Xina Liu, Jinjin Gu, Yu Qiao, and Chao Dong. Reflash dropout in image super-resolution. In *Proceedings of the IEEE/CVF Conference on Computer Vision and Pattern Recognition*, pages 6002–6012, 2022. 2, 7, 13, 17, 18, 19, 20

[41] Simon Kornblith, Mohammad Norouzi, Honglak Lee, and Geoffrey Hinton. Similarity of neural network representations revisited. In *International Conference on Machine Learning*, pages 3519–3529. PMLR, 2019. 15

[42] Alexander Krull, Tim-Oliver Buchholz, and Florian Jug. Noise2void-learning denoising from single noisy images. In *Proceedings of the IEEE/CVF conference on computer vision and pattern recognition*, pages 2129–2137, 2019. 2

[43] Christopher Kulla, Alejandro Conty, Clifford Stein, and Larry Gritz. Sony pictures imageworks arnold. *ACM Transactions on Graphics (TOG)*, 37(3):1–18, 2018. 6

[44] Stamatios Lefkimmiatis. Non-local color image denoising with convolutional neural networks. In *Proceedings of the IEEE conference on computer vision and pattern recognition*, pages 3587–3596, 2017. 2

[45] Stamatios Lefkimmiatis. Universal denoising networks: a novel cnn architecture for image denoising. In *Proceedings of the IEEE conference on computer vision and pattern recognition*, pages 3204–3213, 2018. 2

[46] Jingyun Liang, Jiezhang Cao, Guolei Sun, Kai Zhang, Luc Van Gool, and Radu Timofte. Swinir: Image restoration using swin transformer. In *CVPR*, 2021. 2, 3, 4, 6, 7, 13, 16, 17, 18, 19, 20

[47] Bee Lim, Sanghyun Son, Heewon Kim, Seungjun Nah, and Kyoung Mu Lee. Enhanced deep residual networks for single image super-resolution. In *CVPRW*, 2017. 5

[48] Anran Liu, Yihao Liu, Jinjin Gu, Yu Qiao, and Chao Dong. Blind image super-resolution: A survey and beyond. *IEEE Transactions on Pattern Analysis and Machine Intelligence*, 2022. 2

[49] Ding Liu, Bihan Wen, Yuchen Fan, Chen Change Loy, and Thomas S Huang. Non-local recurrent network for image restoration. *Advances in neural information processing systems*, 31, 2018. 2

[50] Yihao Liu, Anran Liu, Jinjin Gu, Zhipeng Zhang, Wenhao Wu, Yu Qiao, and Chao Dong. Discovering" semantics" in super-resolution networks. *arXiv preprint arXiv:2108.00406*, 2021. 2, 3, 8

[51] Yihao Liu, Hengyuan Zhao, Jinjin Gu, Yu Qiao, and Chao Dong. Evaluating the generalization ability of super-resolution networks. *arXiv preprint arXiv:2205.07019*, 2022. 2, 3, 8

[52] Kede Ma, Zhengfang Duanmu, Qingbo Wu, Zhou Wang, Hongwei Yong, Hongliang Li, and Lei Zhang. Waterloo exploration database: New challenges for image quality assessment models. *TIP*, 2016. 5

[53] Salma Abdel Magid, Zudi Lin, Donglai Wei, Yulun Zhang, Jinjin Gu, and Hanspeter Pfister. Texture-based error analysis for image super-resolution. In *Proceedings of the IEEE/CVF Conference on Computer Vision and Pattern Recognition*, pages 2118–2127, 2022. 3

[54] Julien Mairal, Francis Bach, Jean Ponce, Guillermo Sapiro, and Andrew Zisserman. Non-local sparse models for image

restoration. In *2009 IEEE 12th international conference on computer vision*, pages 2272–2279. IEEE, 2009. 2

[55] Xiaojiao Mao, Chunhua Shen, and Yu-Bin Yang. Image restoration using very deep convolutional encoder-decoder networks with symmetric skip connections. *Advances in neural information processing systems*, 29, 2016. 2

[56] David Martin, Charless Fowlkes, Doron Tal, and Jitendra Malik. A database of human segmented natural images and its application to evaluating segmentation algorithms and measuring ecological statistics. In *Proceedings Eighth IEEE International Conference on Computer Vision. ICCV 2001*, volume 2, pages 416–423. IEEE, 2001. 4, 5, 7, 15, 19

[57] Deepak Pathak, Philipp Krahenbuhl, Jeff Donahue, Trevor Darrell, and Alexei A Efros. Context encoders: Feature learning by inpainting. In *Proceedings of the IEEE conference on computer vision and pattern recognition*, pages 2536–2544, 2016. 3

[58] Tobias Plotz and Stefan Roth. Benchmarking denoising algorithms with real photographs. In *Proceedings of the IEEE conference on computer vision and pattern recognition*, pages 1586–1595, 2017. 2

[59] Tobias Plötz and Stefan Roth. Neural nearest neighbors networks. *Advances in Neural information processing systems*, 31, 2018. 2

[60] Alec Radford, Karthik Narasimhan, Tim Salimans, Ilya Sutskever, et al. Improving language understanding by generative pre-training. 2018. 3

[61] Alec Radford, Jeffrey Wu, Rewon Child, David Luan, Dario Amodei, Ilya Sutskever, et al. Language models are unsupervised multitask learners. *OpenAI blog*, 1(8):9, 2019. 3

[62] Maithra Raghu, Thomas Unterthiner, Simon Kornblith, Chiyuan Zhang, and Alexey Dosovitskiy. Do vision transformers see like convolutional neural networks? *Advances in Neural Information Processing Systems*, 34:12116–12128, 2021. 7, 15

[63] Shuwei Shi, Jinjin Gu, Liangbin Xie, Xintao Wang, Yujiu Yang, and Chao Dong. Rethinking alignment in video super-resolution transformers. *arXiv preprint arXiv:2207.08494*, 2022. 2

[64] Ying Tai, Jian Yang, Xiaoming Liu, and Chunyan Xu. Memnet: A persistent memory network for image restoration. In *Proceedings of the IEEE international conference on computer vision*, pages 4539–4547, 2017. 2

[65] Radu Timofte, Eirikur Agustsson, Luc Van Gool, Ming-Hsuan Yang, Lei Zhang, Bee Lim, Sanghyun Son, Heewon Kim, Seungjun Nah, Kyoung Mu Lee, et al. Ntire 2017 challenge on single image super-resolution: Methods and results. In *CVPRW*, 2017. 5

[66] Mathias Uhlen, Per Oksvold, Linn Fagerberg, Emma Lundberg, Kalle Jonasson, Mattias Forsberg, Martin Zwahlen, Caroline Kampf, Kenneth Wester, Sophia Hober, et al. Towards a knowledge-based human protein atlas. *Nature biotechnology*, 28(12):1248–1250, 2010. 3

[67] Pascal Vincent, Hugo Larochelle, Isabelle Lajoie, Yoshua Bengio, Pierre-Antoine Manzagol, and Léon Bottou. Stacked denoising autoencoders: Learning useful representations in a deep network with a local denoising criterion. *Journal of machine learning research*, 11(12), 2010. 3

[68] Zhendong Wang, Xiaodong Cun, Jianmin Bao, and Jianzhuang Liu. Uformer: A general u-shaped transformer for image restoration. *arXiv preprint arXiv:2106.03106*, 2021. 2

[69] Kaixuan Wei, Ying Fu, Jiaolong Yang, and Hua Huang. A physics-based noise formation model for extreme low-light raw denoising. In *Proceedings of the IEEE/CVF Conference on Computer Vision and Pattern Recognition*, pages 2758–2767, 2020. 1, 2

[70] Zhenda Xie, Zheng Zhang, Yue Cao, Yutong Lin, Jianmin Bao, Zhuliang Yao, Qi Dai, and Han Hu. Simmim: A simple framework for masked image modeling. In *Proceedings of the IEEE/CVF Conference on Computer Vision and Pattern Recognition*, pages 9653–9663, 2022. 2, 3

[71] Fuzhi Yang, Huan Yang, Jianlong Fu, Hongtao Lu, and Baining Guo. Learning texture transformer network for image super-resolution. In *CVPR*, 2020. 2

[72] Yuan Yuan, Siyuan Liu, Jiawei Zhang, Yongbing Zhang, Chao Dong, and Liang Lin. Unsupervised image super-resolution using cycle-in-cycle generative adversarial networks. In *Proceedings of the IEEE Conference on Computer Vision and Pattern Recognition Workshops*, pages 701–710, 2018. 1, 2

[73] Zongsheng Yue, Hongwei Yong, Qian Zhao, Deyu Meng, and Lei Zhang. Variational denoising network: Toward blind noise modeling and removal. *Advances in neural information processing systems*, 32, 2019. 2

[74] Zongsheng Yue, Qian Zhao, Lei Zhang, and Deyu Meng. Dual adversarial network: Toward real-world noise removal and noise generation. In *European Conference on Computer Vision*, pages 41–58. Springer, 2020. 2

[75] Syed Waqas Zamir, Aditya Arora, Salman Khan, Munawar Hayat, Fahad Shahbaz Khan, and Ming-Hsuan Yang. Restormer: Efficient transformer for high-resolution image restoration. In *CVPR*, 2022. 2

[76] Syed Waqas Zamir, Aditya Arora, Salman Khan, Munawar Hayat, Fahad Shahbaz Khan, and Ming-Hsuan Yang. Restormer: Efficient transformer for high-resolution image restoration. In *Proceedings of the IEEE/CVF Conference on Computer Vision and Pattern Recognition*, pages 5728–5739, 2022. 6, 7, 13, 16, 17, 18, 19, 20

[77] Syed Waqas Zamir, Aditya Arora, Salman Khan, Munawar Hayat, Fahad Shahbaz Khan, Ming-Hsuan Yang, and Ling Shao. Multi-stage progressive image restoration. In *Proceedings of the IEEE/CVF conference on computer vision and pattern recognition*, pages 14821–14831, 2021. 2

[78] Jiale Zhang, Yulun Zhang, Jinjin Gu, Jiahua Dong, Linghe Kong, and Xiaokang Yang. Xformer: Hybrid x-shaped transformer for image denoising. *arXiv preprint arXiv:2303.06440*, 2023. 2

[79] Jiale Zhang, Yulun Zhang, Jinjin Gu, Yongbing Zhang, Linghe Kong, and Xin Yuan. Accurate image restoration with attention retractable transformer. *arXiv preprint arXiv:2210.01427*, 2022. 2, 4

[80] Kai Zhang, Yawei Li, Jingyun Liang, Jiezhang Cao, Yulun Zhang, Hao Tang, Radu Timofte, and Luc Van Gool. Practical blind denoising via swin-conv-unet and data synthesis. *arXiv preprint arXiv:2203.13278*, 2022. 2, 5

[81] Kai Zhang, Wangmeng Zuo, Yunjin Chen, Deyu Meng, and Lei Zhang. Beyond a gaussian denoiser: Residual learning of deep cnn for image denoising. *IEEE transactions on image processing*, 26(7):3142–3155, 2017. 1, 2, 6, 7, 13, 14, 16, 17, 18, 19, 20

[82] Kai Zhang, Wangmeng Zuo, and Lei Zhang. Ffdnet: Toward a fast and flexible solution for cnn-based image denoising. *IEEE Transactions on Image Processing*, 27(9):4608–4622, 2018. 2

[83] Lei Zhang, Xiaolin Wu, Antoni Buades, and Xin Li. Color demosaicking by local directional interpolation and nonlocal adaptive thresholding. *Journal of Electronic imaging*, 20(2):023016, 2011. 5, 15, 18

[84] Richard Zhang, Phillip Isola, Alexei A Efros, Eli Shechtman, and Oliver Wang. The unreasonable effectiveness of deep features as a perceptual metric. In *CVPR*, 2018. 5

[85] Yulun Zhang, Kunpeng Li, Kai Li, Gan Sun, Yu Kong, and Yun Fu. Accurate and fast image denoising via attention guided scaling. *IEEE Transactions on Image Processing*, 30:6255–6265, 2021. 2

[86] Yulun Zhang, Kunpeng Li, Kai Li, Bineng Zhong, and Yun Fu. Residual non-local attention networks for image restoration. *arXiv preprint arXiv:1903.10082*, 2019. 2, 6, 7, 13, 16, 17, 18, 19, 20

[87] Yulun Zhang, Yapeng Tian, Yu Kong, Bineng Zhong, and Yun Fu. Residual dense network for image restoration. *IEEE Transactions on Pattern Analysis and Machine Intelligence*, 43(7):2480–2495, 2020. 2

Appendix

A. Details of the Test Noise

We evaluate the generalization performance of the models on six different synthetic noise types to evaluate the generalization performance on the noise out of the training set: (1) **Speckle noise** is a kind of noise that can occur during the acquisition of medical images or tomography images. We use different variances σ^2 to obtain different levels of noise. The *imnoise* function in MATLAB is used for generating Speckle noise. We add multiplicative noise according to the equation $J = I + n * I$, where n is uniformly distributed random noise with mean 0 and variance σ^2, J is the noisy image.

(2) **Poisson noise** is a kind of signal-dependent noise that occurs during the acquisition of digital images. We amplified the noise using different scaling factor α using the equation $J = I + n * \alpha$, where we generate Poisson noise n first, then multiply it by a scaling factor α.

(3) **Spatially-correlated noise** indicates additive Gaussian noise filtered with an average kernel of size 3×3. Different levels indicate different standard deviations σ for the used Gaussian noise. This is to synthesize the complex artifact after denoising using a flawed algorithm.

(4) **Salt & pepper noise**. Different noise levels represent different noise densities, denoted by d. The *imnoise* function in MATLAB is used for generating Salt & pepper noise. This noise can appear during image acquisition as a result of camera imaging pipeline errors.

(5) **Image signal processing (ISP) noise**. Modern digital cameras aim to produce visually pleasing and accurate images that match human perception. The raw sensor data captured by the camera cannot directly produce a usable image, and several post-processing stages are required to convert its linear intensities into the final image [5]. As the original raw image contains noise, the post-processed image exhibits more complex noise. Since there are no adequate real noisy and noise-free image pairs, many denoising algorithms perform poorly on real data due to the gap between synthetic and real noise. In our experiments, we use the default parameter settings of [5] to synthesize ISP noise on RGB images.

(6) **Mixture noise** is obtained by mixing the above different types of noise with different levels. We consider the real-world case where the image suffers from multiple degradations. The order of noise adding is Gaussian noise (variances σ_g^2), speckle noise (variances σ_{s1}^2), Poisson noise (scale α), Salt & pepper noise (density d), speckle noise (variances σ_{s2}^2). Since speckle noise is a multiplicative noise, it will have different effects when used in different positions. It will be multiplied by the noise already existing in the image to obtain complex noise degradation. There are 4 levels:
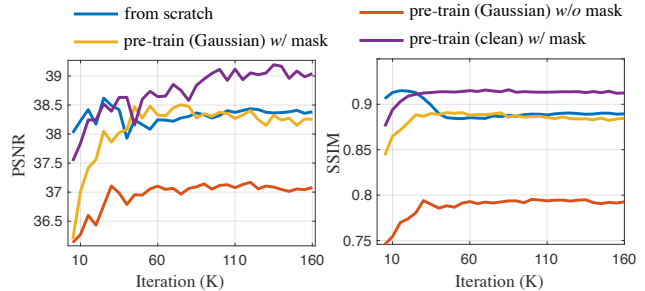
Figure 16. Training curve of different methods validated using our SIDD testset.

ID	Pre-train	SIDD Fine-tune	Masked Traning	PSNR	SSIM	LPIPS
1	Gaus. 15			32.11	0.6606	0.5434
2	Gaus. 15		✓	33.01	0.6999	0.4626
3	None	✓		38.36	0.8879	0.3555
4	Gaus. 15	✓		37.08	0.7920	0.3622
5	Gaus. 15	✓	✓	38.15	0.8822	0.3237
6	Clean	✓	✓	**39.11**	**0.9135**	**0.2614**

Table 4. Masked pre-training for limited paired data. Our method of pre-training on clean images by masked training first and then fine-tuning on target limited dataset yields the best results.

1. $\sigma_g^2 = 0.003$, $\sigma_{s1}^2 = 0.003$, $\alpha = 1$, $d = 0.002$, $\sigma_{s2}^2 = 0.003$;

2. $\sigma_g^2 = 0.004$, $\sigma_{s1}^2 = 0.004$, $\alpha = 1$, $d = 0.002$, $\sigma_{s2}^2 = 0.004$;

3. $\sigma_g^2 = 0.006$, $\sigma_{s1}^2 = 0.006$, $\alpha = 1$, $d = 0.003$, $\sigma_{s2}^2 = 0.006$;

4. $\sigma_g^2 = 0.008$, $\sigma_{s1}^2 = 0.008$, $\alpha = 1$, $d = 0.004$, $\sigma_{s2}^2 = 0.008$;

The noise patterns produced by these four settings are completely different from existing studies.

We also include two real noise types in this work: the Smartphone Image Denoising Dataset (SIDD) [1] and Monte Carlo (MC) rendered image noise [25].

B. Additional Comparisons

Methods for Comparison. We compare our method with several classical methods: DnCNN [81], RIDNet [2], RNAN [86], SwinIR [46], Restormer [76], Dropout [40]. Among them, Dropout [40] was proposed to improve the generalization ability and relieve the overfitting problem. Following [40], we apply the dropout layer with a dropout probability of 0.7 before the output convolutional layer of the baseline model.

Masked Training as Pre-training. In many real-world scenarios, we can only access very limited image pairs for

010_0179_008_S6_03200_00800_5500_L   HQ   Noisy   SwinIR   from scratch   pre-train *w/o* mask   pre-train *w/* mask
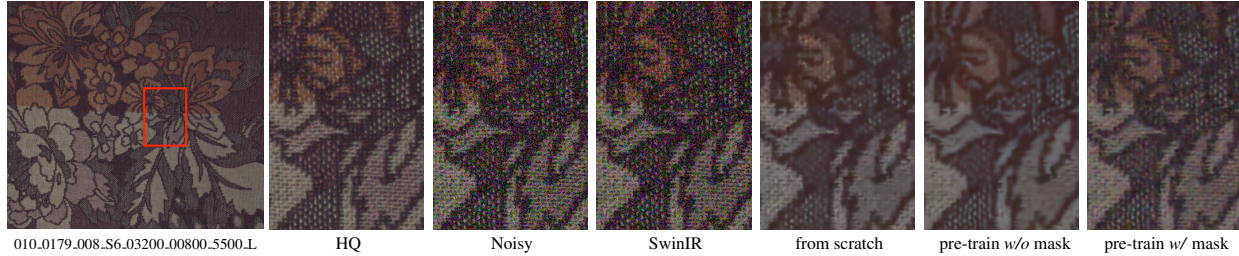
Figure 17. Visual comparison of different methods on real smartphone noise dataset SIDD [1]. "SwinIR" is trained on Gaussian noise, $\sigma = 15$. "from scratch" is trained directly on the target two SIDD training samples. "pre-train *w/o* mask" is pre-trained on Gaussian noise, $\sigma = 15$, and fine-tuned without mask. "pre-train *w/* mask" is pre-trained on clean images and fine-tuned by masked training.
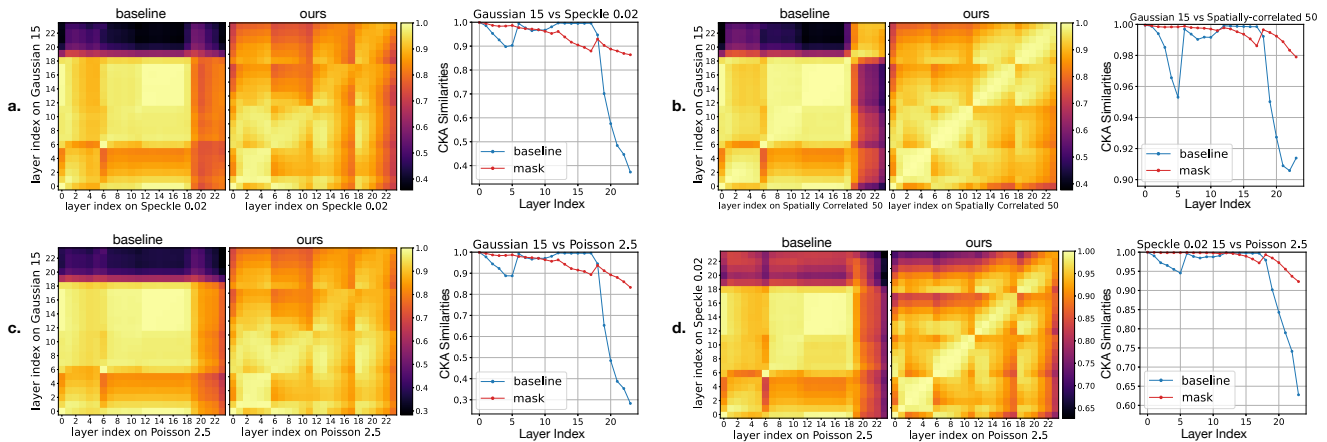
Figure 18. CKA similarity to analyze the representation similarity of network layers.

training. It is not enough to adequately train a denoising network because the network can easily overfit the training data. The performance of the network will be limited if it is trained only on limited data. The pre-training and fine-tuning paradigm may be helpful in this case. One approach is to train the network on the synthetic data first and then fine-tune it on the target data [81], but the performance may also be unsatisfactory because of the gap between the pre-train data and the target data. In this paragraph, we will introduce a practical approach that uses the masked training method for pre-training. We first pre-train the model on clean images with the masked training strategy, and then fine-tune the model on the limited real training samples with the mask. This allows the model to obtain generalization ability even when trained on extremely limited training data. Pre-training on clean images enables the network to learn the content representation of natural images and thus benefits the fine-tuning of target noise. To conduct such experiments, we use images from the SIDD dataset [1]. SIDD contains real noisy images with high-quality clean references. Due to different lighting and different cameras, the noise of the image is also different. It is consistent with the complex noise situation in the real world. In order to simulate a scenario with extremely lim-

ited training samples, the training set only contains two 4K noisy – clean image pairs from SIDD. We also selected one image from each of the ten scenes, for a total of ten images as a test set. Table 4 shows the experiment settings and results. For experiment 3, we directly train the model on the limited training samples. For experiment 4 and 5, we first pre-train the models using Gaussian noise with $\sigma = 15$ and then fine-tune them on target noise. While for experiment 6, we pre-trained the model on clean (noise-free) images with the proposed masked training strategy, and then fine-tuned it on the target training samples. The model pre-trained on clean images using the proposed masked training achieves the best results. This demonstrates the potential of our approach as a new low-level pre-training method. In addition, our method pre-trained on noisy images is not as effective as pre-trained on clean images, which illustrates that our method benefits from learning information about the image's distribution. Visual results are shown in Figure 17. Our method preserves the most texture detail. Figure 16 shows the training curves for different experiments. The numerical performance of the model pre-trained on Gaussian noise and fine-tuned without masking (red line) is generally low and does not increase with training. For the model trained from scratch directly on SIDD (blue line), its PSNR

14

starts to fluctuate at the beginning of training and does not improve any further. Its SSIM even drops with training. This indicates a severe overfitting problem. In contrast, the method using the proposed masked training (purple and yellow lines) can continue to improve the performance during the training process. This indicates that the model has not yet had an overfitting problem. The method pre-trained with clean images (purple line) performs better.

Quantitative Comparison. We provide full numerical results in Table 5, Table 7, Table 6, and Table 8, where we evaluate our method on four benchmark datasets, namely CBSD68 [56], Kodak24 [26], McMaster [83], and Urban100 [36]. Our method outperforms other state-of-the-art models significantly across all noise types. Particularly, we obtain a significant lead in LPIPS performance, suggesting that our results have better human visual perceptual quality.

Additional Visual Results. Figure 19 shows more visual comparisons. The model's performance without masked training is significantly limited over the various noise types. Our model still effectively removes noise when dealing with a variety of noise outside the training set.

C. Additional Analyses of CKA

In the main text, in order to investigate how masked training differs from normal training strategy, we utilize the centered kernel alignment (CKA) [18, 62] to analyze the differences between network representations obtained from those two training methods. In detail, we calculate the representations of two layers $\mathbf{X} \in \mathbb{R}^{m \times p_1}$ and $\mathbf{Y} \in \mathbb{R}^{m \times p_2}$ on the same m data points, with p_1 and p_2 neurons respectively. Gram matrices $\mathbf{K} = \mathbf{X}\mathbf{X}^\top$ and $\mathbf{L} = \mathbf{Y}\mathbf{Y}^\top$ are used to compute CKA:

$$\mathrm{CKA}(\mathbf{K}, \mathbf{L}) = \frac{\mathrm{HSIC}(\mathbf{K}, \mathbf{L})}{\sqrt{\mathrm{HSIC}(\mathbf{K}, \mathbf{K})\mathrm{HSIC}(\mathbf{L}, \mathbf{L})}}$$

where HSIC is the Hilbert-Schmidt independence criterion [41]. Given the centering matrix $\mathbf{H} = \mathbf{I}_n - \frac{1}{n}\mathbf{1}\mathbf{1}^\top$, and centered Gram matrices $\mathbf{K}' = \mathbf{H}\mathbf{K}\mathbf{H}$ and $\mathbf{L}' = \mathbf{H}\mathbf{L}\mathbf{H}$, we have $\mathrm{HSIC}(\mathbf{K}, \mathbf{L}) = \mathrm{vec}\,(\mathbf{K}') \cdot \mathrm{vec}\,(\mathbf{L}')/(m-1)^2$. More CKA results are shown in Figure 18. We first compare the correlation of the features between different noise types. For the baseline model, the correlation between the features of Gaussian noise and other different noises at the deep level is relatively low (a, b, c). Besides, the feature correlation between the noise outside the training set is also low (d). The model using the proposed masked training is able to have a high correlation in all cases. Figure 18 (a) shows the cross-model comparison between baseline and masked training models. We find that a significant difference between the two is that the features of the deeper layers of the

baseline model have low correlations with all layers of our model. This indicates that these two training methods have inconsistent learning patterns for features, especially for the deeper layers. To explore how the model performs on different noise, Figure 18 (b) shows the cross-noise comparison between in-distribution noise and out-of-distribution noise (Gaussian and Poisson noise). For the baseline model, there is a low correlation between the different noise in the deep layers. It shows that the network processes these two types of noise differently for the deep layers. The other types of noise share a similar phenomenon. We suggest that this is because the baseline approach makes the deep layer of the model focus on overfitting the patterns of the training set, which leads to the poor generalization of the deep layers to handle different noise. In our model, the correlation between adjacent layers in our model is high. The proposed masked training forces the network to learn the distribution of the images themselves, which is similar to different types of noise. This allows our method to have a stronger generalization capability.

CBSD68: img_0067 · Salt-and-pepper noise, $d = 0.02$ · DnCNN [81] · RIDNet [2] · RNAN [86] · Restormer [76] · SwinIR [46] · baseline · Masked Training

urban100: img_054 · Speckle noise, $\sigma^2 = 0.016$ · DnCNN [81] · RIDNet [2] · RNAN [86] · Restormer [76] · SwinIR [46] · baseline · Masked Training

kodak24: img_14 · Poisson noise 2 · DnCNN [81] · RIDNet [2] · RNAN [86] · Restormer [76] · SwinIR [46] · baseline · Masked Training

McM: img_2 · Spatially-correlated noise, $\sigma = 45$ · DnCNN [81] · RIDNet [2] · RNAN [86] · Restormer [76] · SwinIR [46] · baseline · Masked Training

kodak24: img_10 · Poisson noise, $\alpha = 1.7$ · DnCNN [81] · RIDNet [2] · RNAN [86] · Restormer [76] · SwinIR [46] · baseline · Masked Training

CBSD68: img_0009 · Mixture noise, level 1 · DnCNN [81] · RIDNet [2] · RNAN [86] · Restormer [76] · SwinIR [46] · baseline · Masked Training

16

Figure 19. Visual comparison.

Speckle noise	$\sigma^2 = 0.02$			$\sigma^2 = 0.024$			$\sigma^2 = 0.03$			$\sigma^2 = 0.04$		
Method	PSNR	SSIM	LPIPS	PSNR	SSIM	LPIPS	PSNR	SSIM	LPIPS	PSNR	SSIM	LPIPS
DnCNN [81]	30.74	0.8281	0.1806	29.31	0.7891	0.2082	27.49	0.7353	0.2533	25.22	0.6620	0.3292
RIDNet [2]	31.01	0.8337	0.1665	29.51	0.7916	0.1944	27.57	0.7331	0.2436	25.17	0.6554	0.3212
RNAN [86]	30.15	0.8101	0.1660	28.59	0.7662	0.1972	26.76	0.7101	0.2449	24.59	0.6377	0.3203
SwinIR [46]	29.64	0.7939	0.1555	28.16	0.7514	0.1851	26.43	0.6981	0.2305	24.37	0.6298	0.3004
Restormer [76]	29.95	0.8135	0.1521	28.84	0.7810	0.1767	27.50	0.7395	0.2113	25.66	0.6839	0.2649
Dropout [40]	29.97	0.8382	0.1709	29.03	0.8041	0.1974	27.77	0.7570	0.2413	26.14	0.6925	0.3110
baseline	29.84	0.8016	0.1778	28.34	0.7608	0.2082	26.56	0.7071	0.2536	24.44	0.6367	0.3242
Ours	**31.22**	**0.8739**	**0.1594**	**30.81**	**0.8617**	**0.1683**	**30.20**	**0.8412**	**0.1849**	**29.10**	**0.8000**	**0.2248**
Poisson noise	$\alpha = 2$			$\alpha = 2.5$			$\alpha = 3$			$\alpha = 3.5$		
Method	PSNR	SSIM	LPIPS	PSNR	SSIM	LPIPS	PSNR	SSIM	LPIPS	PSNR	SSIM	LPIPS
DnCNN [81]	28.41	0.7359	0.2284	24.38	0.5767	0.3887	21.63	0.4571	0.5330	19.65	0.3711	0.6521
RIDNet [2]	28.17	0.7231	0.2215	24.00	0.5546	0.3849	21.34	0.4379	0.5246	19.48	0.3567	0.6397
RNAN [86]	27.55	0.7000	0.2231	23.66	0.5402	0.3783	21.14	0.4263	0.5184	19.33	0.3486	0.6355
SwinIR [46]	27.32	0.6877	0.2081	23.68	0.5398	0.3487	21.17	0.4294	0.4860	19.32	0.3506	0.6059
Restormer [76]	29.22	0.7639	0.1662	26.11	0.6452	0.2608	23.98	0.5613	0.3530	22.55	0.5174	0.4306
Dropout [40]	28.47	0.7601	0.2209	25.61	0.6245	0.3652	23.53	0.5218	0.4986	21.97	0.4454	0.6136
baseline	27.70	0.7040	0.2339	23.85	0.5524	0.3782	21.27	0.4377	0.5109	19.45	0.3550	0.6241
Ours	**30.59**	**0.8510**	**0.1662**	**28.80**	**0.7709**	**0.2488**	**27.04**	**0.6834**	**0.3493**	**25.46**	**0.6039**	**0.4502**
Spatially-correlated	$\sigma = 40$			$\sigma = 45$			$\sigma = 50$			$\sigma = 55$		
Method	PSNR	SSIM	LPIPS	PSNR	SSIM	LPIPS	PSNR	SSIM	LPIPS	PSNR	SSIM	LPIPS
DnCNN [81]	29.63	0.8036	0.3527	28.17	0.7474	0.4192	26.85	0.6898	0.4718	25.70	0.6360	0.5173
RIDNet [2]	28.94	0.7766	0.4109	27.58	0.7189	0.4746	26.39	0.6637	0.5208	25.34	0.6131	0.5580
RNAN [86]	28.86	0.7644	0.3943	27.50	0.7078	0.4532	26.32	0.6542	0.4980	25.28	0.6050	0.5373
SwinIR [46]	28.73	0.7524	0.4056	27.38	0.6951	0.4620	26.20	0.6414	0.5070	25.17	0.5930	0.5458
Restormer [76]	23.42	0.6533	0.4412	23.06	0.6109	0.4783	22.82	0.5709	0.5072	22.59	0.5353	0.5356
Dropout [40]	29.35	0.8173	0.3188	28.27	0.7719	0.3800	27.19	0.7206	0.4400	26.19	0.6694	0.4943
baseline	29.34	0.7834	0.3706	27.82	0.7205	0.4375	26.55	0.6628	0.4878	25.46	0.6118	0.5295
Ours	**29.55**	**0.8296**	**0.2949**	**28.84**	**0.8045**	**0.3358**	**28.05**	**0.7735**	**0.3762**	**27.27**	**0.7388**	**0.4163**
Salt & pepper	$d = 0.002$			$d = 0.004$			$d = 0.008$			$d = 0.012$		
Method	PSNR	SSIM	LPIPS	PSNR	SSIM	LPIPS	PSNR	SSIM	LPIPS	PSNR	SSIM	LPIPS
DnCNN [81]	24.75	0.6785	0.3639	21.15	0.4952	0.5626	17.55	0.2993	0.8196	15.47	0.2066	0.9779
RIDNet [2]	25.19	0.6769	0.3617	21.38	0.4934	0.5498	17.65	0.2969	0.8029	15.60	0.2066	0.9598
RNAN [86]	23.59	0.6416	0.3829	20.42	0.4639	0.5599	17.21	0.2850	0.8048	15.31	0.2006	0.9644
SwinIR [46]	23.42	0.6329	0.3873	20.21	0.4511	0.5710	17.00	0.2688	0.8103	15.14	0.1875	0.9614
Restormer [76]	23.81	0.6384	0.3919	20.99	0.4831	0.5551	19.79	0.3878	0.6512	19.25	0.3257	0.7574
Dropout [40]	27.44	0.7180	0.3041	24.36	0.5557	0.4898	21.01	0.3790	0.7415	19.03	0.2902	0.9047
baseline	25.36	0.6510	0.3694	21.93	0.4747	0.5642	18.42	0.2939	0.8153	16.46	0.2106	0.9656
Ours	**30.52**	**0.8477**	**0.1768**	**28.48**	**0.7681**	**0.2786**	**25.01**	**0.5958**	**0.5039**	**22.48**	**0.4622**	**0.6979**
Mixture noise	**level 1**			**level 2**			**level 3**			**level 4**		
Method	PSNR	SSIM	LPIPS	PSNR	SSIM	LPIPS	PSNR	SSIM	LPIPS	PSNR	SSIM	LPIPS
DnCNN [81]	28.31	0.7514	0.2299	26.53	0.6636	0.3011	23.55	0.5117	0.4522	21.66	0.4162	0.5622
RIDNet [2]	28.13	0.7335	0.2215	26.11	0.6320	0.2971	23.13	0.4776	0.4461	21.34	0.3899	0.5514
RNAN [86]	27.46	0.7090	0.2280	25.67	0.6126	0.2948	22.90	0.4657	0.4369	21.19	0.3826	0.5431
SwinIR [46]	27.44	0.7049	0.2051	25.73	0.6113	0.2682	23.03	0.4689	0.4073	21.29	0.3847	0.5145
Restormer [76]	29.23	0.7859	0.1639	28.22	0.7330	0.1965	25.69	0.6034	0.2894	24.05	0.5257	0.3662
Dropout [40]	28.61	0.7797	0.2071	27.23	0.7039	0.2777	24.96	0.5715	0.4290	23.49	0.4906	0.5324
baseline	28.12	0.7295	0.2259	26.22	0.6346	0.2985	23.28	0.4795	0.4441	21.44	0.3885	0.5463
Ours	**30.31**	**0.8518**	**0.1617**	**29.63**	**0.8251**	**0.1903**	**28.12**	**0.7513**	**0.2732**	**26.91**	**0.6841**	**0.3530**

Table 5. Quantitative comparison on Kodak24 [26].

Speckle noise	$\sigma^2 = 0.02$			$\sigma^2 = 0.024$			$\sigma^2 = 0.03$			$\sigma^2 = 0.04$		
Method	PSNR	SSIM	LPIPS	PSNR	SSIM	LPIPS	PSNR	SSIM	LPIPS	PSNR	SSIM	LPIPS
DnCNN [81]	30.67	0.8254	0.1506	29.24	0.7927	0.1840	27.54	0.7551	0.2269	25.49	0.7095	0.2856
RIDNet [2]	30.77	0.8261	0.1444	29.31	0.7934	0.1757	27.58	0.7551	0.2168	25.49	0.7081	0.2750
RNAN [86]	29.77	0.8066	0.1492	28.32	0.7745	0.1814	26.67	0.7377	0.2224	24.75	0.6932	0.2796
SwinIR [46]	29.17	0.7947	0.1258	27.83	0.7660	0.1524	26.30	0.7322	0.1893	24.46	0.6909	0.2412
Restormer [76]	28.89	0.8005	0.1300	27.95	0.7790	0.1515	26.81	0.7523	0.1807	25.30	0.7173	0.2213
Dropout [40]	28.64	0.8153	0.1416	27.85	0.7852	0.1688	26.89	0.7501	0.2032	25.64	0.7062	0.2525
baseline	28.86	0.7283	0.1353	27.61	0.7014	0.1593	26.15	0.6679	0.1938	24.38	0.6251	0.2437
Ours	**30.33**	**0.8157**	**0.1130**	**30.01**	**0.8016**	**0.1238**	**29.53**	**0.7800**	**0.1412**	**28.66**	**0.7463**	**0.1761**

Poisson noise	$\alpha = 2$			$\alpha = 2.5$			$\alpha = 3$			$\alpha = 3.5$		
Method	PSNR	SSIM	LPIPS	PSNR	SSIM	LPIPS	PSNR	SSIM	LPIPS	PSNR	SSIM	LPIPS
DnCNN [81]	29.13	0.7771	0.1772	25.40	0.6740	0.2915	22.78	0.5910	0.3972	20.86	0.5261	0.4846
RIDNet [2]	29.00	0.7706	0.1681	25.17	0.6636	0.2838	22.59	0.5836	0.3877	20.76	0.5227	0.4730
RNAN [86]	28.13	0.7488	0.1760	24.58	0.6476	0.2897	22.18	0.5710	0.3916	20.44	0.5119	0.4765
SwinIR [46]	27.85	0.7419	0.1468	24.48	0.6459	0.2472	22.12	0.5710	0.3419	20.35	0.5122	0.4229
Restormer [76]	28.74	0.7765	0.1310	25.78	0.6936	0.2082	23.57	0.6296	0.2778	21.94	0.5792	0.3342
Dropout [40]	27.74	0.7699	0.1649	25.56	0.6751	0.2645	23.84	0.5986	0.3558	22.47	0.5377	0.4355
baseline	27.89	0.7024	0.1557	24.51	0.6025	0.2522	22.19	0.5361	0.3427	20.49	0.4761	0.4207
Ours	**30.01**	**0.8016**	**0.1120**	**28.67**	**0.7439**	**0.1683**	**27.23**	**0.6876**	**0.2329**	**25.99**	**0.6347**	**0.2976**

Spatially-correlated	$\sigma = 40$			$\sigma = 45$			$\sigma = 50$			$\sigma = 55$		
Method	PSNR	SSIM	LPIPS	PSNR	SSIM	LPIPS	PSNR	SSIM	LPIPS	PSNR	SSIM	LPIPS
DnCNN [81]	29.92	0.8159	0.2221	28.59	0.7672	0.2718	27.35	0.7160	0.3197	26.23	0.6665	0.3654
RIDNet [2]	29.36	0.7958	0.2608	28.06	0.7433	0.3146	26.90	0.6910	0.3624	25.85	0.6426	0.4056
RNAN [86]	29.16	0.7792	0.2542	27.85	0.7257	0.3053	26.70	0.6751	0.3514	25.68	0.6286	0.3941
SwinIR [46]	29.10	0.7710	0.2498	27.77	0.7165	0.3005	26.61	0.6658	0.3446	25.59	0.6193	0.3876
Restormer [76]	24.46	0.6408	0.2867	23.90	0.6043	0.3217	23.48	0.5723	0.3542	23.18	0.5431	0.3874
Dropout [40]	28.15	0.7946	0.2123	27.32	0.7542	0.2562	26.47	0.7097	0.3021	25.65	0.6649	0.3493
baseline	29.43	0.7731	0.2365	28.05	0.7191	0.289	26.61	0.6532	0.3513	25.82	0.6223	0.3770
Ours	**28.96**	**0.7996**	**0.1952**	**28.36**	**0.7779**	**0.2216**	**27.65**	**0.7529**	**0.2507**	**27.01**	**0.7251**	**0.2827**

Salt & pepper	$d = 0.002$			$d = 0.004$			$d = 0.008$			$d = 0.012$		
Method	PSNR	SSIM	LPIPS	PSNR	SSIM	LPIPS	PSNR	SSIM	LPIPS	PSNR	SSIM	LPIPS
DnCNN [81]	23.53	0.6675	0.3607	20.13	0.4878	0.5403	16.72	0.2966	0.7748	14.73	0.2057	0.9320
RIDNet [2]	24.01	0.6639	0.3581	20.48	0.4864	0.5288	16.93	0.2960	0.7584	14.92	0.2065	0.9131
RNAN [86]	22.62	0.6428	0.3731	19.54	0.4651	0.5374	16.43	0.2854	0.7626	14.59	0.2007	0.9193
SwinIR [46]	22.68	0.6391	0.3580	19.50	0.4581	0.5226	16.32	0.2749	0.7379	14.47	0.1914	0.8889
Restormer [76]	23.04	0.6398	0.3667	20.10	0.4829	0.5207	18.64	0.3555	0.6163	18.34	0.3156	0.6797
Dropout [40]	25.83	0.6771	0.3082	23.04	0.5197	0.4693	19.89	0.3536	0.6918	17.96	0.2709	0.8487
baseline	24.06	0.6224	0.3485	20.87	0.4630	0.5183	17.69	0.2959	0.7378	15.86	0.2156	0.8867
Ours	**29.51**	**0.7929**	**0.1504**	**27.45**	**0.7117**	**0.2476**	**24.03**	**0.5508**	**0.4350**	**21.59**	**0.4313**	**0.5968**

Mixture noise	level 1			level 2			level 3			level 4		
Method	PSNR	SSIM	LPIPS	PSNR	SSIM	LPIPS	PSNR	SSIM	LPIPS	PSNR	SSIM	LPIPS
DnCNN [81]	28.41	0.7627	0.1869	26.88	0.6989	0.2406	24.16	0.5781	0.3564	22.33	0.4877	0.4447
RIDNet [2]	28.38	0.7509	0.1781	26.65	0.6811	0.2337	23.82	0.5558	0.3479	22.03	0.4659	0.4335
RNAN [86]	27.52	0.7285	0.1886	25.99	0.6616	0.2414	23.42	0.5412	0.3510	21.75	0.4533	0.4351
SwinIR [46]	27.57	0.7271	0.1601	26.07	0.6619	0.2050	23.56	0.5453	0.3059	21.86	0.4557	0.3869
Restormer [76]	28.59	0.7674	0.1410	27.53	0.7210	0.1703	25.29	0.6263	0.2462	23.71	0.5578	0.2991
Dropout [40]	27.47	0.7515	0.1694	26.41	0.6924	0.2190	24.58	0.5856	0.3255	23.27	0.5086	0.4079
baseline	28.05	0.7472	0.1665	26.40	0.6810	0.2148	23.70	0.5418	0.3229	21.91	0.4397	0.4061
Ours	**29.91**	**0.8267**	**0.1094**	**29.44**	**0.8111**	**0.1312**	**28.24**	**0.7570**	**0.1870**	**27.15**	**0.7018**	**0.2452**

Table 6. Quantitative comparison on McMaster [83].

Speckle noise

Method	$\sigma^2 = 0.02$			$\sigma^2 = 0.024$			$\sigma^2 = 0.03$			$\sigma^2 = 0.04$		
	PSNR	SSIM	LPIPS	PSNR	SSIM	LPIPS	PSNR	SSIM	LPIPS	PSNR	SSIM	LPIPS
DnCNN [81]	29.90	0.8380	0.1699	28.57	0.8044	0.1982	26.90	0.7610	0.2374	24.84	0.7035	0.2996
RIDNet [2]	30.11	0.8404	0.1597	28.75	0.8044	0.1884	27.03	0.7590	0.2305	24.87	0.6999	0.2927
RNAN [86]	29.36	0.8228	0.1593	27.95	0.7883	0.1872	26.28	0.7451	0.2276	24.28	0.6870	0.2893
SwinIR [46]	28.89	0.8101	0.1602	27.55	0.7774	0.1867	25.98	0.7362	0.2251	24.07	0.6810	0.2849
Restormer [76]	29.16	0.8279	0.1518	28.13	0.8015	0.1742	26.84	0.7667	0.2049	25.17	0.7202	0.2523
Dropout [40]	29.13	0.8447	0.1684	28.28	0.8171	0.1953	27.16	0.7804	0.2347	25.69	0.7311	0.2936
baseline	29.11	0.8122	0.1794	27.75	0.7801	0.2077	26.15	0.7393	0.2465	24.19	0.6837	0.3050
Ours	**30.46**	**0.8777**	**0.1435**	**30.08**	**0.8697**	**0.1511**	**29.49**	**0.8502**	**0.1691**	**28.53**	**0.8169**	**0.2060**

Poisson noise

Method	$\alpha = 2$			$\alpha = 2.5$			$\alpha = 3$			$\alpha = 3.5$		
	PSNR	SSIM	LPIPS	PSNR	SSIM	LPIPS	PSNR	SSIM	LPIPS	PSNR	SSIM	LPIPS
DnCNN [81]	28.13	0.7790	0.1957	24.40	0.6417	0.3284	21.77	0.5295	0.4524	19.83	0.4446	0.5639
RIDNet [2]	28.00	0.7705	0.1878	24.08	0.6199	0.3237	21.50	0.5082	0.4459	19.67	0.4279	0.5542
RNAN [86]	27.38	0.7505	0.1902	23.73	0.6081	0.3201	21.29	0.5003	0.4405	19.51	0.4220	0.5498
SwinIR [46]	27.12	0.7392	0.1849	23.69	0.6049	0.3094	21.27	0.4992	0.4282	19.46	0.4200	0.5393
Restormer [76]	28.68	0.7973	0.1506	25.67	0.6951	0.2361	23.54	0.6167	0.3139	21.55	0.5598	0.3831
Dropout [40]	28.03	0.7953	0.1975	25.42	0.6823	0.3220	23.45	0.5901	0.4366	21.94	0.5182	0.5418
baseline	27.55	0.7517	0.2085	23.92	0.6173	0.3346	21.42	0.5087	0.4510	19.63	0.4259	0.5572
Ours	**30.01**	**0.8656**	**0.1390**	**28.48**	**0.8053**	**0.2072**	**26.84**	**0.7318**	**0.2974**	**25.33**	**0.6616**	**0.3937**

Spatially-correlated

Method	$\sigma = 40$			$\sigma = 45$			$\sigma = 50$			$\sigma = 55$		
	PSNR	SSIM	LPIPS	PSNR	SSIM	LPIPS	PSNR	SSIM	LPIPS	PSNR	SSIM	LPIPS
DnCNN [81]	29.38	0.8304	0.2819	28.02	0.7839	0.3379	26.78	0.7349	0.3864	25.68	0.6880	0.4290
RIDNet [2]	28.74	0.8092	0.3306	27.45	0.7603	0.3865	26.32	0.7122	0.4300	25.31	0.6670	0.4672
RNAN [86]	28.68	0.7983	0.3192	27.39	0.7499	0.3703	26.25	0.7029	0.4122	25.25	0.6591	0.4500
SwinIR [46]	28.56	0.7883	0.3353	27.26	0.7389	0.3853	26.13	0.6918	0.4298	25.13	0.6484	0.4664
Restormer [76]	24.54	0.7076	0.3661	24.17	0.6689	0.4007	23.70	0.6320	0.4348	23.35	0.5978	0.4640
Dropout [40]	28.89	0.8383	0.2580	27.89	0.7999	0.3109	26.90	0.7563	0.3656	25.96	0.7123	0.4135
baseline	29.11	0.8109	0.3071	27.69	0.7578	0.3658	26.48	0.7078	0.4147	25.42	0.6625	0.4537
Ours	**29.08**	**0.8445**	**0.2431**	**28.43**	**0.8242**	**0.2765**	**27.71**	**0.7985**	**0.3127**	**27.03**	**0.7719**	**0.3476**

Salt & pepper

Method	$d = 0.002$			$d = 0.004$			$d = 0.008$			$d = 0.012$		
	PSNR	SSIM	LPIPS	PSNR	SSIM	LPIPS	PSNR	SSIM	LPIPS	PSNR	SSIM	LPIPS
DnCNN [81]	24.39	0.7102	0.3205	20.88	0.5423	0.5032	17.33	0.3499	0.7615	15.27	0.2510	0.9304
RIDNet [2]	24.83	0.7065	0.3165	21.12	0.5400	0.4912	17.44	0.3470	0.7459	15.41	0.2510	0.9096
RNAN [86]	23.32	0.6768	0.3312	20.19	0.5127	0.4970	16.99	0.3343	0.7464	15.12	0.2443	0.9133
SwinIR [46]	23.21	0.6724	0.3416	20.04	0.5035	0.5123	16.84	0.3206	0.7541	14.97	0.2320	0.9190
Restormer [76]	23.58	0.6779	0.3429	20.77	0.5292	0.5016	19.13	0.4143	0.6322	18.37	0.3500	0.7409
Dropout [40]	26.92	0.7433	0.2739	23.97	0.5999	0.4380	20.70	0.4330	0.6832	18.75	0.3431	0.8508
baseline	25.09	0.6879	0.3289	21.71	0.5261	0.5088	18.25	0.3480	0.7621	16.30	0.2594	0.9216
Ours	**29.96**	**0.8558**	**0.1512**	**28.01**	**0.7893**	**0.2295**	**24.69**	**0.6391**	**0.4408**	**22.23**	**0.5174**	**0.6331**

Mixture noise

Method	**level 1**			**level 2**			**level 3**			**level 4**		
	PSNR	SSIM	LPIPS	PSNR	SSIM	LPIPS	PSNR	SSIM	LPIPS	PSNR	SSIM	LPIPS
DnCNN [81]	27.91	0.7876	0.1955	26.28	0.7151	0.2561	23.52	0.5791	0.3825	21.70	0.4867	0.4833
RIDNet [2]	27.80	0.7740	0.1888	25.97	0.6885	0.2510	23.14	0.5463	0.3777	21.38	0.4589	0.4752
RNAN [86]	27.16	0.7543	0.1946	25.52	0.6718	0.2515	22.89	0.5366	0.3711	21.22	0.4532	0.4683
SwinIR [46]	27.10	0.7477	0.1827	25.51	0.6668	0.2378	22.96	0.5363	0.3563	21.29	0.4523	0.4533
Restormer [76]	28.54	0.8091	0.1493	27.50	0.7625	0.1796	25.17	0.6509	0.2599	23.52	0.5729	0.3270
Dropout [40]	28.01	0.8076	0.1841	26.78	0.7455	0.2455	24.70	0.6296	0.3722	23.29	0.5532	0.4672
baseline	27.81	0.7717	0.2022	26.06	0.6916	0.2659	23.27	0.5476	0.3927	21.48	0.4563	0.4886
Ours	**29.74**	**0.8672**	**0.1342**	**29.14**	**0.8466**	**0.1551**	**27.80**	**0.7900**	**0.2231**	**26.62**	**0.7305**	**0.2964**

Table 7. Quantitative comparison on CBSD68 [56].

Speckle noise	$\sigma^2 = 0.02$			$\sigma^2 = 0.024$			$\sigma^2 = 0.03$			$\sigma^2 = 0.04$		
Method	PSNR	SSIM	LPIPS	PSNR	SSIM	LPIPS	PSNR	SSIM	LPIPS	PSNR	SSIM	LPIPS
DnCNN [81]	28.66	0.8207	0.1456	27.28	0.7880	0.1745	25.64	0.7478	0.2138	23.67	0.6962	0.2716
RIDNet [2]	28.73	0.8218	0.1386	27.31	0.7874	0.1683	25.63	0.7457	0.2086	23.63	0.6933	0.2662
RNAN [86]	27.99	0.8047	0.1414	26.60	0.7726	0.1697	25.01	0.7333	0.2085	23.14	0.6826	0.2652
SwinIR [46]	27.50	0.7931	0.1408	26.19	0.7626	0.1683	24.68	0.7256	0.2059	22.88	0.6772	0.2609
Restormer [76]	28.22	0.8100	0.1370	27.17	0.7851	0.1578	25.86	0.7529	0.1874	24.15	0.7106	0.2302
Dropout [40]	27.69	0.8258	0.1516	26.83	0.7981	0.1797	25.78	0.7639	0.2167	24.42	0.7200	0.2693
baseline	27.66	0.7916	0.1611	26.33	0.7617	0.1877	24.80	0.7242	0.2241	22.98	0.6753	0.2772
Ours	**28.97**	**0.8771**	**0.1062**	**28.60**	**0.8642**	**0.1180**	**28.04**	**0.8421**	**0.1421**	**27.12**	**0.8055**	**0.1832**

Poisson noise	$\alpha = 2$			$\alpha = 2.5$			$\alpha = 3$			$\alpha = 3.5$		
Method	PSNR	SSIM	LPIPS	PSNR	SSIM	LPIPS	PSNR	SSIM	LPIPS	PSNR	SSIM	LPIPS
DnCNN [81]	27.72	0.7814	0.1656	24.06	0.6682	0.2738	21.52	0.5807	0.3740	19.65	0.5128	0.4638
RIDNet [2]	27.51	0.7728	0.1600	23.75	0.6536	0.2697	21.27	0.5675	0.3686	19.51	0.5025	0.4561
RNAN [86]	26.88	0.7550	0.1634	23.37	0.6428	0.2682	21.02	0.5593	0.3662	19.30	0.4953	0.4544
SwinIR [46]	26.59	0.7451	0.1586	23.27	0.6392	0.2575	20.95	0.5575	0.3533	19.21	0.4929	0.4426
Restormer [76]	28.39	0.7964	0.1326	25.34	0.7049	0.2043	22.89	0.6266	0.2802	21.25	0.5684	0.3524
Dropout [40]	27.19	0.7928	0.1722	24.82	0.6989	0.2706	22.98	0.6269	0.3607	21.55	0.5698	0.4437
baseline	26.94	0.7511	0.1790	23.45	0.6425	0.2788	21.09	0.5593	0.3712	19.40	0.4936	0.4556
Ours	**28.72**	**0.8710**	**0.1051**	**27.48**	**0.8142**	**0.1668**	**26.04**	**0.7446**	**0.2464**	**24.71**	**0.6845**	**0.3232**

Spatially-correlated	$\sigma = 40$			$\sigma = 45$			$\sigma = 50$			$\sigma = 55$		
Method	PSNR	SSIM	LPIPS	PSNR	SSIM	LPIPS	PSNR	SSIM	LPIPS	PSNR	SSIM	LPIPS
DnCNN [81]	29.87	0.8526	0.1912	28.50	0.8110	0.2371	27.23	0.7677	0.2795	26.09	0.7258	0.3173
RIDNet [2]	29.24	0.8364	0.2216	27.89	0.7908	0.2702	26.68	0.7464	0.3116	25.62	0.7051	0.3464
RNAN [86]	29.07	0.8203	0.2248	27.72	0.7767	0.2674	26.54	0.7351	0.3052	25.50	0.6961	0.3385
SwinIR [46]	28.99	0.8116	0.2360	27.64	0.7678	0.2769	26.46	0.7265	0.3131	25.43	0.6882	0.3455
Restormer [76]	26.38	0.7360	0.2593	25.56	0.7011	0.2902	24.77	0.6686	0.3189	24.06	0.6384	0.3455
Dropout [40]	28.68	0.8529	0.1797	27.78	0.8191	0.2204	26.86	0.7808	0.2635	25.96	0.7411	0.3046
baseline	29.58	0.8440	0.2092	28.11	0.7950	0.2567	26.84	0.7492	0.2974	25.74	0.7076	0.3323
Ours	28.06	**0.8586**	**0.1720**	27.55	**0.8410**	**0.1976**	26.98	**0.8196**	**0.2266**	**26.40**	**0.7951**	**0.2562**

Salt & pepper	$d = 0.002$			$d = 0.004$			$d = 0.008$			$d = 0.012$		
Method	PSNR	SSIM	LPIPS	PSNR	SSIM	LPIPS	PSNR	SSIM	LPIPS	PSNR	SSIM	LPIPS
DnCNN [81]	24.01	0.7372	0.2643	20.55	0.5828	0.4143	17.05	0.4029	0.6335	15.01	0.3062	0.7973
RIDNet [2]	24.56	0.7372	0.2613	20.88	0.5835	0.4062	17.20	0.4023	0.6220	15.16	0.3072	0.7824
RNAN [86]	23.01	0.7132	0.2744	19.87	0.5582	0.4137	16.71	0.3892	0.6223	14.86	0.2999	0.7840
SwinIR [46]	22.90	0.7075	0.2823	19.74	0.5507	0.4215	16.56	0.3790	0.6231	14.71	0.2910	0.7773
Restormer [76]	23.42	0.7145	0.2799	20.53	0.5772	0.4086	18.65	0.4571	0.5308	17.81	0.3967	0.6311
Dropout [40]	26.33	0.7591	0.2326	23.48	0.6279	0.3647	20.29	0.4781	0.5635	18.35	0.3943	0.7181
baseline	24.92	0.7224	0.2667	21.56	0.5752	0.4130	18.11	0.4103	0.6263	16.15	0.3225	0.7840
Ours	**28.58**	**0.8655**	**0.1158**	**26.93**	**0.8074**	**0.1850**	**24.01**	**0.6780**	**0.3530**	**21.75**	**0.5652**	**0.5140**

Mixture noise	level 1			level 2			level 3			level 4		
Method	PSNR	SSIM	LPIPS	PSNR	SSIM	LPIPS	PSNR	SSIM	LPIPS	PSNR	SSIM	LPIPS
DnCNN [81]	27.62	0.7842	0.1656	26.08	0.7221	0.2120	23.41	0.6112	0.3116	21.64	0.5332	0.3907
RIDNet [2]	27.51	0.7725	0.1592	25.75	0.7011	0.2076	23.01	0.5844	0.3080	21.31	0.5099	0.3851
RNAN [86]	26.85	0.7535	0.1651	25.28	0.6866	0.2092	22.75	0.5759	0.3046	21.13	0.5041	0.3813
SwinIR [46]	26.79	0.7475	0.1566	25.26	0.6816	0.1973	22.81	0.5751	0.2878	21.19	0.5040	0.3634
Restormer [76]	28.45	0.8085	0.1269	27.39	0.7665	0.1517	25.03	0.6716	0.2171	23.26	0.5984	0.2749
Dropout [40]	27.22	0.7976	0.1608	26.11	0.7431	0.2077	24.22	0.6484	0.3035	22.91	0.5849	0.3770
baseline	27.47	0.7795	0.1718	25.79	0.7136	0.2191	23.12	0.5931	0.3170	21.38	0.5131	0.3925
Ours	**28.57**	**0.8749**	**0.0995**	**28.08**	**0.8566**	**0.1186**	**26.97**	**0.8053**	**0.1747**	**25.97**	**0.7516**	**0.2337**

Table 8. Quantitative comparison on Urban100 [36].